Chemical characterization and source apportionment of submicron aerosols measured in Senegal during the 2015 SHADOW campaign

Laura-Hélèna Rivellini[1,2] [*], Isabelle Chiapello[2], Emmanuel Tison[1], Marc Fourmentin[3], Anaïs Féron[4], Aboubacry Diallo[5], Thierno N'Diaye[5], Philippe Goloub[2], Francesco Canonaco[6], André Stephan Henry Prévôt[6], and Véronique Riffault[1] [*]

[1]IMT Lille Douai, Univ. Lille, SAGE - Département Sciences de l'Atmosphère et Génie de l'Environnement, 59000 Lille, France
[2]Laboratoire d'Optique Atmosphérique, Université de Lille - CNRS, Villeneuve d'Ascq, 59655, France
[3]Laboratoire de Physico-Chimie de l'Atmosphère, Université du Littoral Côte d'Opale, Dunkerque, 59140, France
[4]Laboratoire Interuniversitaire des Systèmes Atmosphériques, CNRS - Université Paris Est Créteil - Université Paris Diderot, Créteil, 94010, France
[5]Institut de Recherche pour le Développement, M'Bour, Senegal
[6]Laboratory of Atmospheric Chemistry, Paul Scherrer Institute, 5232 Villigen, Switzerland

[*] *Correspondence to*:

Véronique Riffault
Tel.: +33 327 712 604, Fax: +33 327 712 914, e-mail: veronique.riffault@imt-lille-douai.fr

Laura-Hélèna Rivellini
e-mail: laura.rivellini@imt-lille-douai.fr

Abstract. The present study offers the first chemical characterization of the submicron (PM_1) fraction in West Africa at a high time resolution, thanks to collocated measurements of non-refractory (NR) species with an Aerosol Chemical Speciation Monitor (ACSM), black carbon and iron concentrations derived from absorption coefficient measurements with a 7-wavelength aethalometer, and total PM_1 determined by a TEOM-FDMS for mass closure. The field campaign was carried out during four months (March to June 2015) as part of the SHADOW (SaHAran Dust Over West Africa) project at a coastal site located in the outskirts of the city of M'Bour, Senegal. With an average mass concentration of 5.4 µg m^{-3}, levels of NR-PM_1 in M'Bour were three to ten times lower than cities like Paris or Beijing. Nonetheless the first half of the observation period was marked by intense but short pollution events (concentrations higher than 15 µg m^{-3}), sea breeze phenomena and Saharan desert dust outbreaks (PM_{10} up to 900 µg m^{-3}). During the second half of the campaign, the sampling site was mainly under the influence of marine air masses. The air masses on days under continental and sea breeze influences were dominated by organics (36-40%), whereas sulfate particles were predominant (40%) for days under oceanic influence. Overall, measurements showed that about 3/4 of the total PM_1 were explained by NR-PM_1, BC and Fe (a proxy for dust) concentrations, leaving ~1/4 for other refractory species. A mean value of 4.6% for the Fe/PM_1 ratio was obtained. Source apportionment of the organic fraction, using Positive Matrix Factorization (PMF) highlighted the impact of local combustion sources, such as traffic and residential activities, which contribute on average to 52% of the total organic fraction. A new

organic aerosol (OA) source, representing on average 3% of the total OA fraction, showed similar variation as non-refractory particulate chloride. Its rose plot and daily pattern pointed out to local combustion processes, that is to say two open waste burning areas located about 6 and 11 km away from the receptor site and to a lesser extent a traditional fish smoking place. The remaining fraction was identified as oxygenated organic aerosols (OOA), a factor

5   that prevailed regardless of the day type (45%) and was representative of regional but also local sources due to enhanced photochemical processes.

1 Introduction

Atmospheric aerosols play a key role in the Earth's radiative forcing, by interacting with incoming solar and

10   outgoing terrestrial radiations (direct effect) and influencing cloud formation, growth and lifetime (indirect effects). Important uncertainties related to such effects remain, as reported in the IPCC reports (IPCC, 2007, 2013). Besides, several epidemiological and toxicological studies (Brook et al., 2004; Kelly and Fussell, 2012) also highlight the sanitary impacts of particulate matter (PM) depending on their size, chemical composition and exposure time. In 2012, around 3.7 million deaths were attributed to cardiovascular and respiratory diseases caused by outdoor PM

15   exposure (Brauer et al., 2012). As a response, the World Health Organization (WHO) established in 2006 air quality thresholds for PM: a daily average of 25 (respectively 50) μg m^{-3} and a mean annual limit of 10 (respectively 20) μg m^{-3} for $PM_{2.5}$ (PM with diameter < 2.5 μm) (PM_{10}) (WHO, 2006). During past decades, high-time resolution monitoring instruments have been implemented in Europe within the ACTRIS (Aerosols, Clouds, and Trace gases Research Infrastructure network) program, in America with the IMPROVE (Interagency Monitoring of Protected

20   Visual Environments) network (Prenni et al., 2016; Schurman et al., 2015) or more recently in Asia, in order to better characterize fine particles. Yet, the African continent remains poorly documented in terms of particulate pollution. Several studies in West Africa (mostly sub-Saharan regions) have focused on the coarse fraction, since this area is strongly influenced by natural sources, especially the Sahara desert that injects high amounts of mineral aerosols into the atmosphere (e.g Chiapello et al., 1995). Among field campaigns, a large effort was performed on aerosol

25   measurements during the AMMA (African Monsoon Multidisciplinary Analysis) program carried out between 2002 and 2010, with intensive observation periods in 2006 (Redelsperger et al., 2006). During the dry season (extending from November to May) the transport of desert dust (DD) and biomass burning (BB) aerosols were observed to occur into two layers, one dominated by DD close to the surface (< 1 km), the one containing BB aerosols being located at a higher altitude, between 2 and 4 km (Haywood et al., 2008; Osborne et al., 2008). During one of the

30   AMMA special observing periods (SOP) (February 2006), a chemical characterization of particles at the ground level was performed near M'Bour (Senegal) using filter sampling and individual particle analysis (Deboudt et al., 2010; Flament et al., 2011). The analysis evidenced both internal and external mixing of DD, sea salt (SS) and carbonaceous aerosols (Deboudt et al., 2010) within the surface layer. The compositions of the coarse (2-10 μm) and fine (< 2 μm) fractions were established at the surface; DD dominated the coarse fraction while organic matter was

35   the major constituent of the fine one. Similar analysis were performed on samples collected during aircraft flights (Formenti et al., 2008a) to determine the chemical composition of aerosols at different altitudes. The altitude layer

was mainly composed of BB and DD external mixture (Chou et al., 2008; Hand et al., 2010). From January to March 2006 (AMMA SOP-0), several types of events from mixtures of DD and BB aerosols to pure mineral dust events were identified based on column aerosol retrievals from AERONET sun/sky photometer measurements in M'Bour, Senegal (Derimian et al., 2008). Other field campaigns such as POLCA ("POLlution des Capitales Africaines" on the Pollution of African Capitals) highlighted the presence of anthropogenic sources of aerosols linked to the strong demographic growth, limited traffic pollution regulations and traditional activities such as slash-and-burn cultivation that generates huge amounts of BB aerosols (Liousse et al., 2010). Its aim was rather on the chemical characterization of $PM_{2.5}$, especially Black Carbon (Doumbia et al., 2012), and the impact on health (Val et al., 2013). Nevertheless, to the best of our knowledge, only one other study has performed on-line and real-time chemical characterization of major PM_1 constituents on the African continent. It was conducted during one year in Welgegund, South Africa, at a site influenced by anthropogenic sources and devoid of mineral dust or marine contribution (Tiitta et al., 2014). Their results have shown that the submicron fraction was dominated by organic and sulfate species, with a chemical composition similar to those encountered in megacities like Beijing (Sun et al., 2012), Mexico (Salcedo et al., 2006) or Pittsburgh (Zhang et al., 2005). Such a pattern differs strongly from those recently measured in European urban cities, where the main submicron pollutants are organic and nitrate species (Petit et al., 2015; Schlag et al., 2015).

In this study we offer the first insight of a real-time, continuous and long-term chemical characterization of PM_1 in West Africa, performed in M'Bour, Senegal from March to June 2015 as part of the first intensive observation period (IOP-1) of the SHADOW (SaHAran Dust Over West Africa) field campaign. An Aerosol Chemical Speciation Monitor (ACSM) was chosen for the quantification and chemical characterization of non-refractory submicron particles, the instrument being better suited for unattended and long term monitoring. Parallel measurements of BC and total PM_1 allowed for mass closure. This paper reports the chemical composition of the submicron fraction and the temporal behaviour of particulate species. The sources and processes responsible for the concentrations encountered at the M'Bour site over the period have been assessed using source-receptor modeling as well as dynamic meteorological measurements parameters and back-trajectory analyses.

2 Instrumentation and methods

2.1 Site description and the SHADOW campaign

The sampling site is located within the '*Institut de Recherche et Développement*' (IRD) facility in M'Bour (14°23'38''N, 16°57'32''W), Senegal. This site, located near the seashore at 80 km south of Dakar (Figure 1), is known to be under the influence of Saharan dust, sea salt, and biomass burning during part of the dry season (from December to March). The site may also be affected by regional anthropogenic emissions from surrounding cities including M'Bour and Dakar, and from traditional fish-smoking activities and open waste burning areas. These potential aerosol source locations are reported in Figure 1. The M'Bour station, as part of the international AERONET network (Holben et al., 1998) is routinely equipped with active and passive remote sensing instruments for cloud, aerosol and meteorological monitoring (CIMEL sun/sky photometer, CIMEL micro-Lidar, fluxmeters and

a weather station). Since the AMMA campaigns in 2006, M'Bour is also one of the three ground-based stations of the "Sahelian Dust Transect" where PM_{10} mass concentrations are measured continuously (every 5 minutes) thanks to a Tapered Element Oscillating Microbalance (TEOM) (Marticorena et al., 2010; Kaly et al., 2015).

SHADOW main objectives are to better determine the physical and chemical properties of particles in this region largely influenced by high concentrations, and to establish a link between them, the atmospheric dynamics and the aerosol load and optical properties. A large panel of high-performance instruments has therefore been added to the AERONET station (Holben et al., 1998) implemented in M'Bour since 1996 (Derimian et al., 2008). Optical and microphysical aerosol measurements (results not presented) were also performed on site by active and passive remote-sensing instruments, like the LiLAS LIDAR (Bovchaliuk et al., 2014; Veselovskii et al., 2016) and a PLASMA airborne sun photometer (Karol et al., 2013). PM_{10} in situ optical measurements at the surface were carried out by a mono-wavelength aethalometer and a nephelometer. Fine and coarse particle size distributions were recorded by a GRIMM optical particle counter, while ground and airborne filter sampling were collected through a 4-stage DEKATI cascade impactor to be analyzed off-line by individual particle analysis. A Doppler Lidar was implemented to improve our understanding of the atmospheric dynamics between the surface and up to 2-3 km over the IRD station in order to provide more accurate micro-meteorological information.

The online chemical composition measurements presented here were acquired during IOP-1, which took place from March 20 to June 22, 2015. Results discussed in this paper focus on the chemical characterization of surface PM_1. The instruments presented hereafter were set up in an air-conditioned room located underneath the flat roof of the IRD main building. Co-located wind speed and direction were measured by an ultrasonic anemometer (model USA-1, METEK GmbH) deployed on the rooftop (about 12 m above ground).

2.2 Instrumentation

2.2.1 ACSM

The chemical characterization of non-refractory submicron particles (NR-PM_1), that is to say material vaporizing around 600°C under close-to-vacuum conditions, was performed on-line and in real time every 30 minutes by an ACSM (Aerodyne Research Inc.). This instrument is based on the same principle as the aerosol mass spectrometers (AMS), without providing size distribution information. A full description of the instrument is presented in Ng et al. (2011). Basically it is composed of an aerodynamic lens that focuses the particle beam (with vacuum aerodynamic diameters below 1 µm) and directs it through three vacuum chambers, the last one being a detection chamber in which particles are vaporized by impaction on a surface heated at 600°C. Non-refractory species, such as organic matter (OM), sulfate (SO_4^{2-}), nitrate (NO_3^-), ammonium (NH_4^+) and non-refractory chloride (Chl), are vaporized at this temperature and then ionized by electron impact (70 eV). Particles are then detected by mass spectrometry thanks to a residual gas analyser (RGA). Because of a simplest operating system and the use of a quadrupole mass spectrometer, the instrument has lower time-resolution and sensitivity but remains better suited for long-term monitoring. A $PM_{2.5}$ cut-off inlet (URG Cyclone 2000-30EH, Chapel Hill, NC, USA) was placed on the roof at the entrance of the sampling line with a primary flow of 3 LPM and vertically connected to the instrument. A Nafion dryer (PD-200T-12 MPS, Perma Pure) upstream of the inlet reduces the sample relative humidity (RH). Particle

losses were evaluated using the Particle Loss calculator (Von der Weiden et al., 2009) and were inferior to 2%
between 50 nm and 1 μm.

Several calibrations were performed with ammonium nitrate, ammonium sulfate and ammonium chloride individual
solutions (at 0.005 mol L^{-1} in purified water) prior to IOP-1. An average of all previous calibrations with this
5   instrument gives a mean NO$_3$ response factor (RF) of 3.63×10^{-11} and mean relative ionization efficiencies (RIE) of
5.72, 0.58 and 2.26 for ammonium, sulfate and chloride, respectively (see Supplementary Information S1 – Figure
S1(a-d) and Zhang et al., in prep., for more details). Organic and nitrate RIE default values of 1.4 and 1.1,
respectively, were used (Canagaratna et al., 2007). Detection limits in μg m^{-3} were determined by Ng et al. (2011) to
be 0.284 for ammonium, 0.148 for organic matter, 0.024 for sulfate, 0.012 for nitrate and 0.011 for chloride. The
10 ACSM intercomparison which took place in Paris during winter 2013 has also allowed to determine expanded
reproducibility uncertainties of 15, 9, 28 and 36% for NO$_3$, OM, SO$_4$ and NH$_4$ mass concentrations, respectively
(Crenn et al., 2015). In addition to the relative ion transmission efficiency correction applied using a naphthalene
internal standard, the Collection Efficiency (CE) due to particle losses induced by an incomplete vaporization and/or
transmission through the aerodynamic lens was also determined for the whole dataset. Those parameters are mainly
15 influenced by particle shape (size, sphericity) and acidity, ammonium nitrate fraction and RH in the sampling line.
Middlebrook et al. (2012) have developed a correction algorithm based on AMS datasets which is applied on ACSM
mass concentrations and which considers both RH and aerosol chemical composition to obtain a time-dependent
correction of CE values ranging from 0.45 to 0.83 (Figure S1e). Nonetheless due to the presence of the Nafion dryer
at the entrance of the instrument no RH corrections were necessary as RH values were below 30%. A minor fraction
20 (3.2%) of the data was excluded from the dataset due to unstable parameters, which were generally observed after
restarting the instrument following power outages.

2.2.2 AE33 aethalometer

Real-time measurements of aerosol absorption were performed every minute by a seven-wavelength (370, 470, 520,
590, 660, 880 and 950 nm) aethalometer (AE33, Magee Scientific Inc.). The instrument was equipped with a PM$_1$
25 impactor inlet (BGI model SCC-0.732, Waltham, MA, USA) and sampled at 5 L min^{-1}. The aethalometer principle is
based on the measurement of light transmission through a filter onto which aerosols deposit. The attenuation is then
converted into an aerosol absorption coefficient σ_{aer} for each wavelength. BC concentrations are retrieved by
applying a specific mass absorption cross section of 7.77 m^2 g^{-1} to the absorption coefficient at 880 nm. The AE33
instrument uses internal corrections based on the Weingartner et al. (2003) algorithm to account for multiple
30 scattering by the filter and a dual spot technology (Drinovec et al., 2015) to compensate the loading effect. Even if
DD absorption is limited at 880 nm, its occurrence in high concentrations on site might cause an overestimation of
BC concentrations derived from absorption measurements. The method developed by Fialho et al. (2005, 2006,
2014) was used to correct BC concentration data from mineral dust interference. This method is further explained in
section II.3.2.

2.2.3 Other instruments

To achieve mass closure in the submicron fraction and account for the expected refractory material (mineral dust and sea salt), ambient air was sampled at 16.7 L min^{-1} through a PM$_{10}$-inlet (Thermo Fisher Scientific Inc.) mounted on a PM$_1$ cyclone (SCC 2.229, BGI Inc., Waltham, MA). Gravimetric measurements of the total mass concentrations

5 were performed every 6 minutes using a TEOM operating at a temperature of 30°C and equipped with a filtered dynamic measurement system (TEOM-FDMS 1405-F, Thermo Scientific) that can account for semi-volatile material by maintaining temperature under 30°C and relative humidity (RH) below 25 %, as described by Grover et al. (2005). Some data had to be discarded, mainly due to high temperatures encountered during dust events leading to FDMS failure to maintain proper operating conditions.

10 Micro-meteorological parameters (wind speed and direction) at the surface (~10 m high) were obtained from 15-minutes accumulation (at 20 Hz) with an ultrasonic anemometer (model USA-1 by METEK GmbH) with a resolution of 0.01 m s^{-1} and 1°, respectively. A weather station (Campbell Scientific) provided precipitation, RH and temperature data every 10 min.

2.3 Analysis strategy

15 ### 2.3.1 Classification of air masses

The station of M'Bour is under the influence of a typical Sahelian climatic cycle composed of a dry and wet season. The dry season is generally defined from November to April and corresponds to a period for which no significant precipitation is recorded (Kaly et al., 2015). The period from May to October, defined as the wet season, corresponds to the period when precipitation is measured, although significant precipitation is generally limited to a few months,

20 i.e. between July and September in M'Bour during which heavy rain and thunderstorms occur (Kaly et al., 2015). The site is influenced by two important wind flows: the Harmattan conditions, with winds coming from North to North-East (N-NE, 0-45°) during the dry season, and the monsoon conditions during the wet season associated to winds from South-West to North-West (SW-NW, 225-315°). Our study taking place from March to June allowed for the observation of both the late part of the dry season (March-April) and the beginning of the wet season (May-June).

25 During IOP-1 two main prevailing directions were found (Fig. 2a). The first one corresponds to an oceanic influence characterized by surface winds coming from West-South-West to North-West (210-300°) with a total frequency of 56% and wind speeds between 2 and 4 m s^{-1}. The second predominant direction is observed for winds originating from NW to NE (300 to 60°) with a total frequency of around 42% and similar wind speeds (2-4 m s^{-1}). The remaining wind sector (60-210°) is a negligible fraction (2%) (Fig. 2a). The maximum wind speed, 6.8 m s^{-1}, was

30 measured on June 21, 2015, with values above 6 m s^{-1} recorded between 2 and 6 a.m. and associated to SW direction. Our measurements during IOP-1 are generally consistent with monthly average frequencies of M'Bour surface wind directions reported by Kaly et al. (2015) between 2006 and 2010. Indeed, their climatology has shown that spring months are generally influenced by winds coming predominantly from two main sectors, North to East (0-90°, prevailing in March-April) and North-West to South-West (315-225°, dominant in May-June).

35 Each sampling day of IOP-1 was classified according to the locally measured surface wind directions. Three categories of days were indeed identified: (i) days exclusively under northern (N) trade wind influences, i.e. within ±

Atmospheric
Chemistry
and Physics
Discussions

45° of the North (0°) direction, associated with continental influence, have been defined as "continental" (Fig. 2b);(ii) days dominated by westerly winds corresponding to oceanic air masses have been classified as "marine" days (Fig. 2d); (iii) an intermediate category called "sea breeze" days has been observed during which measurements show winds coming from the NE before 2 pm, then shifting from the N to W directions between 2 and 7 pm, and

5   returning to the NW in the evening (Fig. 2c). This phenomenon has been previously observed in M'Bour during the AMMA campaigns as reported by Derimian et al. (2008), Léon et al. (2009) and Deboudt et al. (2012). In summary, among the 91 days of IOP-1, 19% were classified as continental days, 32% as sea breeze days and 49% as marine days. The frequent occurrence of marine days can be explained by the transition from dry to wet season from April to June in the Sahelian region (Redelsperger et al., 2006; Slingo et al., 2008).

10   **2.3.2 Interpretation of absorption measurements**

M'Bour being largely under the influence of mineral dust, a possible overestimation of the amount of BC derived from absorption coefficients measured by the aethalometer (due to DD absorbing properties at shorter wavelengths) has to be considered (Bond and Bergstrom, 2006). These interferences may be enhanced during the dry season by internal mixture of BB and DD, as encountered and evidenced during AMMA by Deboudt et al. (2010) at the surface

15   and by Hand et al. (2010) and Paris et al. (2010) at higher altitude. Consequently, BC absorption coefficients have been recalculated following the method developed by Fialho et al. (2005, 2006, 2014) in order to obtain BC concentrations unbiased by DD influence. It consists in a deconvolution of the wavelength-dependent aerosol absorption coefficient over time, $\sigma_{aer}(\lambda, t)$, into two terms that take into account DD and BC contributions, through the following equations:

20   $$\sigma_{aer}(\lambda, t) = \sigma_{BC}(\lambda, t) + \sigma_{DD}(\lambda, t)$$
(1)

where $\sigma_{BC}(\lambda, t)$ and $\sigma_{DD}(\lambda, t)$ are BC and DD absorption coefficients, respectively, which can be expressed as a function of the species concentrations $\langle C_i(t) \rangle$:

$$\sigma_{BC}(\lambda, t) = K_{BC}\lambda^{\alpha}\langle C_{BC}(t)\rangle$$
25   (2)

$$\sigma_{DD}(\lambda, t) = K_{DD}\lambda^{\beta}\langle C_{DD}(t)\rangle$$
(3)

K_{BC} and K_{DD} are empirical constants depending of instrument characteristics, and α and β are respectively BC and DD absorption exponents. α and β values of - 1 and - 4, respectively, have been determined in the visible range (from

30   470 to 660 nm) by Fialho et al. (2014) with a dataset acquired in the Cape Verde Islands located at approximately 500 km from our sampling site.

Fialho et al. (2006) have replaced dust by iron in order to calculate an iron concentration from dust absorption:

$$K_{Fe}\langle C_{Fe}(t)\rangle = K_{DD}\langle C_{DD}(t)\rangle$$
(4)

35   Indeed, DD absorption is known to be mainly influenced by the iron content (Lafon et al., 2006) even if this element presents rather low mass contribution to the mineral dust total mass. As mentioned by Fialho et al. (2014), this

method allows to estimate elemental iron concentrations only in the absence of brown carbon. The m/z 60 signal ($C_2H_4O_2^+$, fragment characteristic of levoglucosan from biomass burning) was mostly absent of the ACSM dataset during IOP-1, representing on average only 0.003 (0.007 and 0.012 for the 95th and 99th percentiles, respectively, see Figure S5) of the total OM, which is identical to the threshold value of 0.3% suggested by Cubison et al. (2011) to

5   assess the presence of BB aerosols. This point is discussed further in the source apportionment results, in which we tend to attribute m/z 60 emissions to other sources. A few data points (less than 1% of the dataset), under the influence of other combustion processes from specific local activities that may cause a bias in the deconvolution algorithm, have been excluded to derive Fe concentrations (see further discussion in section III.2.2).

Combining Eq.(4) with Eq.(1, 2 and 3) leads to the following expression:

10        $$\frac{\sigma_{aer}(\lambda,t)}{\lambda^\alpha} = K_{BC}\langle C_{BC}(t)\rangle + K_{Fe}\langle C_{Fe}(t)\rangle\, \lambda^{(\beta-\alpha)}$$

       (5)

Eq. (5) can be plotted as a linear equation at each time t to determine the intercept at the origin, a(t), and the slope, b(t). BC and Fe concentrations are then derived using $K_{BC} = 14.625$ μm m^2 g^{-1} in Eq. (6) and $K_{Fe} = 0.234$ μm^4 m^2 g^{-1} in Eq. (7), respectively:

15        $$\langle C_{BC}(t)\rangle = \frac{a(t)}{K_{BC}}$$

       (6)

       $$\langle C_{Fe}(t)\rangle = \frac{b(t)}{K_{Fe}}$$

       (7)

2.3.3 Positive Matrix Factorization (PMF)

20   The PMF model is a statistical source-receptor model developed by Paatero and Tapper (1994), largely employed in source apportionment of atmospheric pollutants when the source profiles and contributions are not known *a priori*. In this study, PMF was applied on the ACSM organic and chloride mass spectra by using the Multilinear Engine (Paatero and Tapper, 1999) and the version 5.3 of the Source Finder (SoFi) described in Canonaco et al. (2013) and operated with IgorPro 6.37 (Wavemetrics). PMF is based on a bilinear model described by the following equations:

25        $$X = GF + E$$

       (8)

       $$x_{ij} = \sum_{k=1}^{p}(g_{i,k}f_{k,j}) + e_{i,j}$$

       (9)

where X, corresponding to model entries, represents the matrix of mass fragment spectra measured, and G and F are

30   matrices of a *k*-factor concentration time series and m/z profile, respectively, where *i* denotes the time step and *j* the mass fragment. The number of factors *p* is formerly determined by the user. The residual matrix E, containing the unexplained fraction of the PMF solution, is minimized by iterations of the model using the Q function:

       $$Q = \sum_i \sum_j \left(\frac{e_{ij}}{s_{ij}}\right)^2$$

       (10)

Atmospheric
Chemistry
and Physics
Discussions

where s_{ij} represents the measurement uncertainties of fragment j at time i. The Q value is then normalized by Q_{exp}, representing the degrees of freedom of the model solution. This normalization is used as an indicator for the solution reliability. Thus a ratio Q/Q_{exp} equal to one means that both variability and uncertainties are totally explained by the model.

5 ### 3 Results and discussion

3.1 Chemical characterization and temporal behavior

3.1.1 NR-PM$_1$, PM$_1$ and PM$_{10}$ mass concentrations

As previously mentioned, Senegal is widely influenced by DD events transported from arid and semi-arid regions of Sahara and Sahel. Moreover, M'Bour being a coastal site, the influence of sea salt (SS) particles on the measured
10 aerosol mass concentrations may be significant. Thus, the contributions of these two aerosol types, in both the coarse and fine fractions of aerosol, have been investigated. PM$_1$ chemical mass closure was checked for all day types by subtracting from the TEOM-FDMS measurements the mass concentrations of species determined by ACSM (NR-PM$_1$) and aethalometer (BC + Fe); the fraction of unaccounted material therefore corresponded to DD and SS contributions.

15 Figure 3a shows the mass concentration time series of NR-PM$_1$ measured by ACSM, total PM$_1$ by TEOM-FDMS, and PM$_{10}$ by TEOM during IOP-1. It must be noted that total PM$_1$ data acquired between March 28 and April 10 had to be invalidated due to instrument overheating during a dust storm event when the outside temperature reached 42°C and PM$_{10}$ concentrations exceeded 600 µg m^{-3}.

The temporal evolutions of the three aerosol fractions do not show any particular correlations (the highest correlation
20 coefficient is obtained between the PM$_1$ and PM$_{10}$ mass concentrations with r = 0.39 for n = 2666). The weak correlation (r = 0.26, n = 2946) between NR-PM$_1$ and PM$_1$ might be explained by the contribution of refractory material (DD and SS) to the total PM$_1$, while the absence of correlation (r = 0.08, n = 3424) between NR-PM$_1$ and PM$_{10}$ was expected, as well as the low average contribution (8%) of NR-PM$_1$ to PM$_{10}$. Indeed, the coarse fraction of aerosol (PM$_{10}$) at this site is dominated by DD and SS (Flament et al., 2011). NR species represent on average 71%
25 of the total PM$_1$, which underlines the significant influence of refractory material in the fine fraction of aerosol measured at M'Bour. During IOP-1, as shown in Figure 3b, despite an important variability (values ranging between 4 and 25%) submicron particles (both refractory and non-refractory fractions) represent on average 11% of the PM$_{10}$ fraction whatever the day type. This pattern has already been observed at other sites influenced by Saharan emissions, and consequently under the influence of DD like Granada (Titos et al., 2015) or Cape Verde (Pio et al.,
30 2014).

Despite similar orders of magnitude between the values of NR-PM$_1$ and total PM$_1$, their ratio exhibits different trends depending on day type (Figure 3c). When comparing PM$_1$ and NR-PM$_1$ concentrations for marine days, NR species appeared to account for most of the PM$_1$ fraction over IOP-1 (slope: 0.71, r = 0.82, n = 452), suggesting a minor influence of sea salt in the PM$_1$ fraction. This conclusion is consistent with the analysis of Flament et al. (2011)
35 during the AMMA SOP-0 in M'Bour, with a reported PM$_2$ fraction composed of 18 to 77% of DD and less than 20%

Atmospheric
Chemistry
and Physics
Discussions

of soluble ions (dominated by NaCl). Additionally for continental and sea breeze scatter plots also reported in Figure 3c, the discrepancies between NR- and total PM_1 mass concentrations are higher (slopes of 0.49 and 0.56, respectively), underlying that continental air masses – predominant during those days – carried additional refractory material such as DD in the submicron fraction. The unaccounted fraction (determined as the difference between the

5   gravimetrically measured PM_1 mass concentration and the sum of chemical species from ACSM and aethalometer measurements) corresponds to 27%, 26% and 16% of the PM_1 mass for continental, sea breeze and marine days, respectively (see Figure S2). A more significant difference could have been expected for continental compared to other days, but this might be explained by the absence of PM_1 mass measurements during the more intense dust events, as mentioned previously. Nevertheless, these results stress the need to apply Fialho et al. (2014)

10   deconvolution in order to separate DD and BC absorption contribution.

3.1.2 Estimation of absorbing compound concentrations in PM₁

Fe and BC concentrations obtained after correction led to averaged values of (0.55 ± 0.85) and (0.36 ± 0.37) µg m^{-3}, respectively, over the whole IOP-1 dataset. The deconvolution led to an average decrease of 45% of BC concentrations (factor of 2.2), which is much higher than the 11% decrease observed by Doumbia et al. (2012) in

15   Dakar where local BC sources are predominant. In our study the decrease even reached 83% under the influence of Saharan dust events and therefore the influence of DD on absorption measurements could never be neglected. As depicted in Figure 4, BC concentrations hardly exceeded 3 µg m^{-3}, except throughout punctual and short-term episodes during which they reached higher values, with a half-hourly average maximum of 3.6 µg m^{-3} reached on April 2, 2015. The higher concentrations can be attributed to local anthropogenic combustion processes as BC

20   concentrations present a significant correlation (r = 0.79) with the ACSM m/z 57 combustion tracer. BC concentrations measured in M'Bour are on average much lower than those measured in Dakar during POLCA (Doumbia et al., 2012), where BC yearly average was (10.5 ± 3.5) µg m^{-3}. The lower concentrations measured here can be explained by the differences in sampling site type and population with the IRD center being located at the outskirts of the city of M'Bour (180 000-200 000 inhabitants) area while the site in Dakar (about 3 million

25   inhabitants within the metropolitan area) was located in an urban area. It can be noted that the range of BC concentrations (0.01-3.6 µg m^{-3}) obtained during IOP-1 in M'Bour is within the same order of magnitude than the one reported by Liousse et al. (2010) for the rural site of Djougou, Benin between Dec. 2005-Feb. 2006 (0.4-8.2 µg m^{-3}).

Fe concentrations estimated from PM_1 absorption measurements are considered as an indicator of DD in the fine

30   fraction. The following comparisons were carried out only on coincident measurements, due to missing data in the PM_1 and PM_{10} datasets, corresponding to lower average concentrations of Fe (0.39 and 0.53 µg m^{-3} for the PM_1 and PM_{10} data comparison, respectively). Although a weak correlation (r = 0.55) was found between Fe and total PM_1 concentrations, Fe concentrations showed higher correlations with PM_{10} (r = 0.70, see Figure 4). This could be explained by DD domination in the coarse fraction, while the fine fraction is mainly driven by NR and BC species

35   during most of the IOP-1 (Figure 3c). As depicted in Figure 4, most of the low iron concentrations were related to days under marine influence, while the highest Fe concentrations (> 8.0 µg m^{-3}) are generally associated with

Atmospheric
Chemistry
and Physics
Discussions

continental and sea breeze days. These maxima also coincide with PM_{10} highest concentrations (> 400 µg m^{-3}) and confirm iron as a constituent of mineral dust emitted by the Saharan and Sahel regions.

Fe contributions to PM_{10} estimated in M'Bour (average Fe/PM_{10} ratio of 0.51% over IOP-1 and 0.89% for continental days) are in excellent agreement with the ~1% of elemental iron in the PM_{100} fraction reported by Joshi et

5   al. (2017) for a DD sample collected at the same location in 2015 after a dust storm. It is however significantly lower than the average content of 11-12% of elemental iron estimated by Formenti et al. (2008) in the PM_{40} dust fraction for samples collected at the ground level in Banizoumbou (Niger). Nonetheless they measured for the same samples an averaged iron concentration of 10 µg m^{-3}, in the same order of magnitude as our maximum concentration of 11.2 µg m^{-3} in PM_1. Besides, Lafon et al. (2006) measured a total iron content of 6 to 8% in PM_{10} bulk samples collected

10   in Niger and Cape Verde, while Moreno et al. (2006) observed a 4% contribution of iron oxides in western Saharan soil samples. Concerning the finer fraction, a mean value of 4.7% was obtained for the Fe/PM_1 ratio over IOP-1 and 7.7% for continental days. The latter value is very close to the 8% of iron content (relative to all oxide mass) observed by Lafon et al. (2006) in the fine mode dust of Nigerian soil samples.

15   **3.1.3 PM_1 average chemical composition**

Table 1 reports ACSM measurements performed at M'Bour between March 20 and June 22, 2015, as well as other field campaigns carried out worldwide. This study shows an average value of 5.4 µg m^{-3} for NR-PM_1 with a maximum half-hourly average of 68.3 µg m^{-3}. The total PM_1 mean concentration (including BC and Fe) is 8.2 µg m^{-3} (maximum half-hourly average: 143 µg m^{-3}), a value which is about 10 times lower than the PM_{10} mean

20   concentration of 103.5 µg m^{-3} over the same period. This PM_{10} average is consistent with the range of monthly averages reported by Kaly et al. (2015) at M'Bour for the March-June period of 2006-2010 (between 63 and 126 µg m^{-3}). When compared to similar studies conducted around the world, M'Bour clearly appears much less polluted than megacities like Beijing (Sun et al., 2012) or Paris area during winter (Petit et al., 2014). The mean NR-PM_1 measured at M'Bour is close to the only other value reported in Africa for Welgegund, South Africa (Tiitta et al.,

25   2014), regional background sites such as MontSec, Spain (Ripoll et al., 2015) or during summer in Paris with an average of 4.5 µg m^{-3} (Petit et al., 2015).

The average NR-PM_1 chemical composition measured in M'Bour was composed of OM (39%), SO_4 (35%), NH_4 (15%) and NO_3 (9%), which is again rather similar to what was observed in South Africa by (Tiitta et al., 2014). Indeed, the OM and SO_4 predominance has been also observed in the majority of cities where ACSM (see Table 1)

30   and AMS (Zhang et al., 2007) campaigns were implemented. Nonetheless, during winter, some European sites like Paris (Petit et al., 2015), Cabauw (Schlag et al., 2015) or Zurich (Lanz et al., 2010) present a fine fraction mainly dominated by nitrate and organic species. In our case these differences could be explained both by the semi-volatile nature of NH_4NO_3 combined with the limited use of fertilizers that prevent NH_3 emissions and ammonium nitrate formation, and more sources of SO_2 such as marine DMS oxidation processes.

35   Figure 5 represents the average contributions of NR-PM_1 species, BC and Fe in PM_1 over the entire IOP-1 and more specifically for continental, sea breeze and marine days. Total PM_1 pie charts, including unaccounted-for aerosol

species obtained by chemical mass closure, have been reported in the supplementary material section (Figure S2). Figure 5 shows that although an almost equal proportion of organic and sulfate species (31 and 32% respectively) was measured on average over the whole IOP-1, strong differences regarding day types can be highlighted: continental and sea breeze days present similar averaged compositions, with a major contribution of OM (36-40%)

5   followed by SO_4 with 21-24%. Similarities between the two profiles are probably due to a longer influence of northern wind compared to western ones during sea breeze days. On the other hand, for marine days the dominant fraction is sulfate (40%) while OM averaged contribution decreased to 25%. These changes could be explained by (i) oceanic air masses known to carry higher amount of sulfate species from the oxidation of dimethylsulfide (DMS) and organosulfur gases (Charlson et al., 1987; Fitzgerald, 1991) and (ii) long-range transport of polluted air masses from

10   the continent, carried back to M'Bour through oceanic air masses. BC and Fe from anthropogenic and continental origins, respectively, are also less abundant during marine days compared to continental/sea breeze days with fractions decreasing from 7 to 3% and 14-16% to 3%, respectively.

Comparable dynamics was already observed at M'Bour during AMMA SOP-0. For instance, Haywood et al. (2008) highlighted that BB aerosols carried in altitude (~3 km) from the African continent to the Atlantic Ocean were then

15   driven back through south-westerly winds. Similar contributions have been observed in Welgegund (Tiitta et al., 2014) where PM_1 measured during the dry season were dominated by OM (57%), followed by SO_4 (16%) and BC (10%), and the wet season marked by high contributions of SO_4 (42%) and lower contributions of OM and BC (35 and 4%, respectively). In M'Bour, we obtained a significant correlation (r = 0.74, Figure S7) between the OM and BC time series and an average BC/OM ratio of 0.15, whatever the day type, suggesting similar emission sources and

20   therefore pointing to continental origins either directly linked to combustion processes, as both species displayed a more important contribution during continental and sea breeze days, or due to the mixing of anthropogenic emissions with biogenic precursors or secondary organic aerosols (SOA).

Aerosol acidity can be considered as an indicator of the age of particles as they will get neutralized during their stay in the atmosphere. In order to estimate the degree of neutralization of ACSM inorganic species, NH_4 measured

25   concentrations (as NH_2^+, NH_3^+ and NH_4^+ ions) are compared to predicted ones, which are equal to the amount of NH_4 required to fully neutralize sulfate, nitrate and chloride anions according to the following equation (Zhang et al., 2007):

$$NH_{4,pred} = M(NH_4) \times \left(2 \times \frac{SO_4^{2-}}{M(SO_4^{2-})} + \frac{NO_3^-}{M(NO_3^-)} + \frac{Cl^-}{M(Cl^-)} \right)$$

(10)

30   with SO_4^{2-}, NO_3^- and Cl^- the mass concentrations of inorganic species in µg m^{-3} and M(X) their molecular weights (NH_4 18; SO_4 96; NO_3 62; and Cl 35.5 g mol^{-1}).

The slope obtained between NH_4 measured and predicted (1.02, r = 0.92; see Figure S3a) underlined that most of inorganic species are neutralized over IOP-1, and additionally that there is no strong bias in the calibration values used for ACSM measurements. Nonetheless, a few points digress from the 1:1 line indicating partially neutralized

35   species (as mentioned above). Points significantly above the 1:1 ratio suggest the presence of NH_4 under other forms than $(NH_4)_2SO_4$, NH_4NO_3 and NH_4Cl. As these points also correspond to higher levels of OM, BC and chloride, circled in red (Figure S3b), they might be related to nitrogen-containing species associated with combustion

processes at low RH (<50%; Figure S3a), where chlorine could come from the combustion of sea salt and/or chlorine-containing materials such as plastics.

3.1.4 Variations of PM_1 chemical species

Figure 6 displays the 30-minute temporal variability of $NR-PM_1$ species during IOP-1. At such a timestamp a total of 13 pollution events – characterized by $NR-PM_1$ concentrations exceeding a threshold value of 15 µg m^{-3}, corresponding to three times the average – were detected. In terms of chemical composition, the highest average - over the whole IOP-1- concentrations were obtained for OM and SO_4 with respective values of 2.12 and 1.85 µg m^{-3} (n = 3931). Moreover OM concentrations could present a high variability over short periods, like on May 12, 2015 when OM jumped from 0.9 to 61.7 µg m^{-3} over an interval of 30 minutes, while the sum of other $NR-PM_1$ species remained below 10 µg m^{-3}.

OM and SO_4 daily fractions exhibit opposite trends, with periods dominated by OM (> 30%) at the beginning of IOP-1 and from May 20 to June 8, 2015, corresponding to days under continental or sea breeze influences. OM concentrations encountered during these periods are generally related to punctual intense episodes, suggesting an influence linked to emissions by rather local anthropogenic activities rather than long-range transport sources. Periods from April 25 to May 21 and after June 9, 2015, associated with oceanic air masses, are dominated by SO_4 (> 30%), with generally more moderate concentrations and less intense peaks, except for May 13th 2015, with $NR-PM_1$ reaching its maximum at 68 µg m^3.

The daily profiles of all identified PM_1 species and meteorological parameters (wind speed, temperature and wind roses) are presented in Figure 7 according to day types. Strong similarities can be observed between the continental and sea breeze daily profiles (Fig. 7a-b), both presenting a morning peak around 8 am marked by a distinct rise in OM (> 4 µg m^{-3}) and BC (~1 µg m^{-3}) concentrations and to a lesser extent in NH_4 and chloride concentrations. Continental and sea breeze daily profiles also show a common peak at 8 pm, less intense than the morning one, but characterized by an increase in OM and BC. It can be noticed that this evening peak is less pronounced for continental days (OM ~ 3.5 µg m^{-3} and BC ~ 0.7 µg m^{-3}) than for sea breeze days (OM ~ 4.5 µg m^{-3} and BC ~ 0.9 µg m^{-3}). As mentioned previously, the BC/OM ratio is on average of 0.13-0.14 for sea breeze and continental days (see Figure S7) but during the morning and evening peaks these ratios can reach a maximum of ~0.25 meaning that BC emissions are enhanced during these hours. A specific pattern of continental days is a peak measured at noon for OM and BC concentrations (constant BC/OM ratio ~ 0.16), probably combining local emissions and reduced dispersion due to dynamic phenomena as suggested by the slight wind speed decrease. On the other hand, for sea breeze days a peak occurring at 3 pm, with an intense increase in OM, a moderate one in SO_4 and almost no variation of BC (ratio of 0.1), coincide with the sea breeze establishment (discernible through wind plots and the slight drop in temperature). BC for continental and sea breeze daily profiles show a maximum intensity of 1.1 µg m^{-3} for the continental morning peak (8 am), a value which is quite consistent with maximal hourly concentrations (up to 4 µg m^{-3}) measured at 8 am, 4 pm and 8 pm in M'Bour by Deboudt et al. (2010). These peaks are measured for air masses coming from the continent and correspond to traffic and/or cooking hours. Chloride peaks associated to intense OM

and BC ones tend to confirm combustion sources for these species, as previously observed during winter in Beijing by Sun et al. (2013).

The marine averaged daily profiles show a very distinctive pattern, compared to continental/sea breeze days (Fig. 7a), and are characterized by a sharp decrease of OM, BC and Fe, with nitrate, ammonium and chloride presenting rather constant profiles, while sulfate exhibits a higher and almost constant concentration of 2.4 µg m^{-3}. This pattern as well as the sulfate peak associated with the sea breeze tends to confirm the regional transport of sulfate to M'Bour through oceanic air masses. It is noticeable that for marine days, OM and BC profiles reached maximum concentrations of 2.5 and 0.35 µg m^{-3} during the night (between 8 pm and 2 am), in coincidence with low wind speed (Fig. 7d). Thus, this night time increase of concentrations measured for marine days might be due to lower dilution of aerosols species from local emissions. The results obtained at M'Bour for marine days are in agreement with those reported by Topping et al. (2004) in Korea, with inorganic species such as SO_4, NO_3 and NH_4 increasing significantly during days under marine influence.

In Figure 7b, Fe and BC profiles showed distinctive behaviors depending on day types. As expected, both profiles for marine days are characterized by very low concentrations of both BC and Fe in comparison to those measured for sea breeze and continental days. In the latter cases, a major difference can be observed for Fe concentrations which are almost twice higher than BC ones. Fe exhibits an additional intense peak around 3 pm and concentrations above 1.5 µg m^{-3} from noon to 8 pm during continental days, which can be attributed to the intense dust events occurring around the end of March and on April 10th when comparing average and median profiles. These patterns suggest a transport of BC and DD (through Fe) by continental air masses – from the areas north and north-east of M'Bour. Most probably air masses loaded in DD coming from the Saharan region (Fe continental profile) are then enriched in BC during their transport above cities. Nonetheless local traffic activities may also be a non-negligible source of dust through resuspension processes, which would also explain the synchronized peaks of BC and Fe observed for continental profiles even when excluding desert dust events.

3.2 Origins and sources of aerosols

3.2.1 Geographical origins of chemical species

As observed previously, most of the winds reaching M'Bour during IOP-1 were associated with the north and west sectors, carrying respectively air masses from the continent and the ocean, with an averaged wind speed of 2.6 m s^{-1}. These results are consistent with the five-year measurements of wind direction reported by Kaly et al. (2015) in M'Bour for the dry season. Figure 8 presents pollution roses obtained combining the time series of the different PM_1 components and co-located surface wind direction/speed measurements, thus offering a first insight into the geographical origins of chemical species. Similar spatial origins can be observed for several species; in particular, OM, BC and Chl maximum concentrations are rather associated with north-east (NE) winds during morning peaks and north-west (NW) winds at the end of the day (Fig. 7), pointing out to a common origin of the higher concentrations observed for these species, that would be linked to combustion processes due to the presence of BC.

Figure 8 also highlights an oceanic origin for some OM (with moderate intensity), SO_4 (as already observed in Fig. 5), NO_3 and NH_4. There is no clear trend linked to the wind speed (slower along the coast and higher when

perpendicular to it), meaning particulate chemical species are rather transported or formed above the ocean than directly emitted by sea spray (Ovadnevaite et al., 2012). Emissions of DMS and organosulfur gases by microorganisms (as mentioned previously) could explain part of the SO_4 and OM concentrations observed when the site is under western influence. These species may also be released by anthropogenic activities in distant cities like

5 Dakar, whose emissions may be carried toward the ocean and brought back to M'Bour by western winds. A long-term PM_{10} chemical characterization conducted in Cape Verde by Fomba et al. (2014) has also shown that marine air masses were mostly composed of sulfate (10% on average) rather than organic matter (3.5%) but the proportion in PM_1 is more balanced.

Regarding the iron pollution rose plot reported in Figure 8, maxima are measured when the site is under the influence

10 of NE winds. For such directions we also observe maximum values of the total PM_1 concentrations (> 60 µg m^{-3}), which correspond to the April 10, 2015, most probably a resuspension event following previous dust storms, as observed on PM_1 and Fe concentrations time series (reported respectively on Figure 3 and 4).

3.2.2 Source apportionment

PMF was first applied without constraints on the whole IOP-1 organic database and then separately on continental,

15 sea breeze and marine extracted datasets (see also Supplementary Information Appendix S4). Three to ten factors were tested and for each run, only solutions with a normalized Q/Q_{exp} ratio close or inferior to 1 were taken into account. Mass spectra were compared to reference profiles for identification and the consistency with daily profiles was checked. Without any constraints applied to the model, one or two factors identified as oxygenated organic aerosols (OOA, dominated by the CO_2^+ fragment at m/z 44) were easily retrieved for all datasets. An unknown factor

20 with peaks at m/z 58, 60, 83 and 91 appears for the whole IOP-1 when the number of factors increases (and is mixed with one of the OOA in the reduced datasets). This factor was associated with one of the OOA for the continental, sea breeze and marine 4-factor unconstrained solutions (Appendix S4, Figure S4.1). Besides, the model encountered difficulties to separate hydrocarbon-like (HOA) from cooking-like (COA) organic aerosol for the entire IOP-1 dataset and the continental and marine days. Both COA and HOA share similar m/z peaks at 27, 41, 55 (C_nH_{2n-1}) and

25 29, 43, 57 (C_nH_{2n+1}) that correspond to hydrocarbon fragmentation. Nonetheless, they can be differentiated based on 41/43 and 55/57 ratios, more important for COA (Fröhlich et al., 2015a; Mohr et al., 2012), while HOA presents more specific and intense peaks at 69-71. Moreover under continental influence, they tend to be emitted from the same wind directions corresponding to the urbanized area from NW to NE. A good separation with characteristic factor profiles was nonetheless obtained for sea breeze days which present a more variable dynamics, with 4 factors

30 identified, namely HOA, COA, as well as more oxidized and less-oxidized OOA (mixed with the unknown factor) (Appendix S4, Figure S4.1c). The unknown factor presents a rose plot and a daily profile consistent with local emissions from the open waste burning areas of Gandigal (NW) and Saly Douté (NE) and a fish-smoking area also located in the NE of M'Bour (Appendix S4, Figure S4.2), hence it has been designated as LCOA (Local Combustion Organic Aerosol). Since the behavior of Chl had also been suspected to come from the same sources, PMF solutions

35 adding the m/z 36 signal in the input matrix were investigated, and a solution is presented in supplementary (Appendix 6). No biomass burning OA (BBOA) profile appeared neither in our unconstrained (up to 10 factors) runs,

nor when HOA and COA were themselves constrained. Furthermore, local practices tend to use dry leaves and branches to feed livestock rather than as combustion fuel, and cooking in the urban area is mainly done on gas stoves. IOP-1 occurring at the transition between dry to wet seasons, the possibility of long-range emissions of BB from Savannah fire, like the one observed for example in South Africa (Tiitta et al., 2014) and northern Australia

5   (Milic et al., 2016), or even other BB regional sources, was not discarded at first. Therefore, an average BBOA profile (Ng et al., 2011b) was used to constrain the PMF solution with different a-values. Using a rather strong constraint of a = 0.3 led to a satisfactory BBOA profile but either stable solutions presenting a mixture between LCOA and part of the OOA factor but no COA, or when LCOA, OOA and COA were well separated, the BBOA profile presented missing fragments and a high run-to-run instability. Moreover, solutions for more moderate

10 constraints (a ≥ 0.5) led to a BBOA profile with unusually low or missing important fragments (such as m/z 60) and an increasing correlation with COA (Crippa et al, 2013). Besides, the important photochemistry observed on site coupled with levoglucosan (m/z 60, 73) fast reactivity under photo-oxidative conditions (Hennigan et al., 2010) might lead to a fast transformation of BBOA into SOA (which would appear as an OOA factor in our PMF solution). Finally, additional in situ or remote sensing optical instruments specifically implemented for the SHADOW

15 campaign, such as ground-based and airborne sunphotometers or the LILAS multiwavelength Mie-Raman lidar (Veselovskii et al., 2016), did not detect the presence of BB aerosol influence. For all these reasons, we decided not to constrain BBOA in our final solutions. In order to refine the solution, and due to the possible specificity of local emissions, the PMF model was run with mild constraints on the primary factor profiles observed in the different unconstrained runs (see Fig. S.4.1) that is to say COA (Crippa et al., 2013) and HOA (Ng et al., 2011b) using the a-

20 value approach with 30 to 90% of freedom (0.3 < a < 0.9) as explained in Canonaco et al. (2013). Indeed HOA are generally emitted by diesel or fuel exhaust, although in rural cities they have also been related to cooking activities (Sun et al., 2012). It has also been reported that African fuels supplied directly by Western company-owned petrol stations present higher levels or sulfur and polyaromatics, and that others are generally a mixture of refinery intermediate products and other (mostly unknown) chemicals, which could hamper the finding of a satisfactory

25 solution. The robustness of the optimal solution was checked by 50 random seed iterations.

A final constrained solution of 4 factors is presented in Figure 9 through their respective mass spectra with associated pollution rose plots and daily profiles for continental, sea breeze and marine days.

The three primary (POA) factors linked to anthropogenic activities, that is to say HOA, COA, and LCOA corresponded to 18, 30 and 3% of the organic fraction, respectively. HOA and COA contributions to the OA fraction

30 tend to be more important for continental and sea breeze days with respectively 21-24% and 24-31% than for marine days (11-20%), while LCOA slightly increases from 2 to 7%. The HOA profile is well correlated with BC (r = 0.79) and m/z 57 (r = 0.98). No specific external tracers have been identified nonetheless COA temporal variability appeared to correlate well with BC (r = 0.73). The HOA rose plot shows marked peaks in the directions of the two open waste burning areas and of the fish-smoking area located northeast of the site in the outskirts of M'Bour. COA

35 main origin in the northwest corresponds to the touristic area of Saly where a number of restaurants are located. BC concentrations previously linked to OM species present close correlations with both HOA and COA but this might be explained by the correlation of 0.82 between both time series suggesting concomitant emissions between traffic and

cooking sources. The variability depicted by their continental and sea breeze daily profiles (Fig. 9b) highlights anthropogenic emissions of COA and HOA with pronounced peaks during morning and evening (0.46 to 0.55 µg m^{-3}) corresponding to human activities. The COA and HOA profiles present an additional peak after 11 am, reaching a maximum around noon then decreasing after 2 pm for continental days. The COA, OOA – and to a much lower

5   extent, the HOA – sea breeze profiles differed from the continental ones by a delay in the midday peak which rises only after 2 pm. This difference could be explained by anthropogenic aerosols emitted in the morning, then transported toward the ocean, and carried back on site through sea breeze phenomena. A similar pattern could have been expected from HOA, but the low concentrations observed suggest faster oxidation processes occurring over the ocean which would contribute to the higher OOA peak. Both COA and HOA factors present low background

10   concentrations during marine days.

As for LCOA which is a very small fraction of the total OA, the fact that it nonetheless consistently appears in the PMF analysis under both unconstrained and constrained conditions, suggests a specific behavior uncorrelated with other sources. Its robustness has been tested under various starting conditions (50 seed iterations) and through rotational ambiguity exploration (F-peak tested between -5 and +5 with a step of 0.5). Despite the fact that Chl

15   species were presenting similar wind sectors origins, its correlation with LCOA remains low (r = 0.44) while LCOA presents higher correlation with m/z 36 and 58 (r = 0.55 and 0.84, respectively). This is mainly due to the influence of refractory chloride (NaCl) in our Chl measurements; which has been observed through m/z 35 negative values likely resulting from a slow vaporization both during filter and non-filter measurements (Nuaaman et al., 2015). Nonetheless m/z 36 (HCl$^+$) was mostly positive (0.03 ± 0.03, see Figure S5) confirming that non-sea salt chloride

20   was also detected. Indeed, if sea salt was predominant in LCOA, NaCl could explain the m/z 58 and 60 signals, but one would have expected a maximum on marine days, whereas LCOA rose plot clearly points out toward the local combustion areas already mentioned previously, and also identified in the chloride rose plot (Figure 8). Although coal combustion used for cooking has been identified as a potential source of chloride emissions (Ianniello et al., 2011; McCulloch et al., 1999), this practice has not been observed in the area. However, chloride species may be

25   emitted from household waste burning/smoldering, for which particle-bound polychlorinated dibenzo-p-dioxins and dibenzofurans (PCDD/Fs) and polychlorinated biphenyls (PCBs) have been measured in previous studies (Gullett et al., 2001; Lemieux et al., 2004; Tue et al., 2016; Zhang et al., 2009); or from sea salt particles subject to high-temperature combustion processes (since this factor is also observed to a lesser extent in the direction of the fish-smoking area).

30   Additionally, the measured NH$_4$ was higher than the predicted one in the directions of the waste burning areas - especially from the North-East (Figure S3b), also suggesting the formation of nitrogen-containing compounds that could lead to R-N$^+$ or R-NO$^+$ fragments at these same masses although high-resolution measurements would be needed to confirm this hypothesis. LCOA also present its most intense peaks in the morning (0.04 µg m^{-3}) and some more moderate in the evening (< 0.03 µg m^{-3}) for continental and sea breeze daily profiles, characteristics of point

35   sources and/or local emissions. These may be linked to the start of the fires in the morning for the open waste burning areas and an evening increase of the OM due to temperature drop that would shift the partitioning of semi-volatile species toward the particulate phase. On the contrary its marine profile shows constant but higher

concentrations all day long (~0.03 µg m^{-3}) with an increase after 8 am, which explains the slightly higher contribution to the OA fraction for the latter.

OOA are often considered as secondary organic aerosols (SOA) formed through gas-conversion processes of Volatile Organic Compounds (VOCs) or photochemical oxidation of primary OA emitted by biogenic (such as plants

5   or algae) and/or anthropogenic sources. The hot temperatures and intense solar irradiation encountered in the region enhance these processes and can explain the major contribution (45%) observed for the OOA factor during IOP-1. Its profile showed intense peaks at m/z 18 and 44 (f_{44} = 0.36) and low 43/44 ratios (0.04), which underlined the high level of oxidation characteristic of aged particles, and presented a correlation of 0.88 with the OOA averaged profile reported by Ng et al. (2011). In our study, the temporal variability of OOA shows a higher correlation with NO_3 than

10 SO_4 (r = 0.56 against r = 0.24). As NO_3 species are generally semi-volatile and associated with less aged air masses (Mohr et al., 2012), OOA might not be only emitted by long distant sources. This is highlighted by daily continental and sea breeze profiles rising around 8 am, noon and 8 pm which emphasize direct emission of oxidized organic aerosols from anthropogenic activities. Also, it has been mentioned previously that NO_3 might not be locally emitted (Figure 8) and OOA highest concentrations being associated with wind speeds above 3 m s^{-1}, we attribute also a

15 regional origin to this factor. Both the OOA correlation with NO_3 and the fact that its daily cycles progressively increase/decrease with sunrise/sunset suggest an important and fast photochemistry (Robinson et al., 2007). The OOA rose plot shows rather similar concentrations regardless of wind sectors, even if some concentrations superior to 1.5 µg m^{-3} are connected to western wind influences (Figure 9). This oceanic origin is also highlighted by OOA sea breeze profile, which shows a maximum of 0.7 µg m^{-3} reached around 3 pm (Figure 9). It indicates that this SOA

20 formation is enhanced during OA transport over the ocean which under specific atmospheric conditions can be initiated by chlorine atoms (Hallquist et al., 2009). OOA increasing during daytime regardless of day type, their high oxidation level and important contribution to OA, especially during marine days (62%), support emissions by regional sources.

Previous observations of OM from daily filter measurements in the PM$_2$ fraction during AMMA SOP-0 were

25 associated maximum values with winds coming from the coast (NW) and the ocean (W) (Flament et al., 2011) and attributed to emissions by local sources and cities along the Senegalese coast, suggesting they could originate from wood burning, cooking and dry leaf/grass burning. Only considering biomass burning and fossil fuel combustion as contributing to the absorption measurements during their field campaign in Dakar, Doumbia et al. (2012) also reported 12% of biomass burning emitted by regional sources against 88% by fossil fuel. Our measurements over a

30 large period of four months at high-time resolution suggest, as mentioned before, that biomass burning from local sources is rather negligible in the M'Bour area during the transition period from dry to wet seasons. Cooking, traffic and other local combustion sources such as traditional fish smoking and household waste burning have been identified as the primary local anthropogenic sources of OM.

4 Conclusions

35 The deployment of high time resolution instruments at the West African coastal site of M'Bour (Senegal) during four months of the 2015 dry season allowed to investigate the temporal variability and chemical composition of the

poorly characterized PM_1 aerosols in this region. The average $NR-PM_1$ concentration (5.4 µg m^{-3}) was relatively low, comparable to levels generally reported in rural environments and also close to the one observed at a South African site. Although marine influence was dominant, various dynamic conditions were encountered during the campaign, with intense dust events, sea breeze phenomena and several anthropogenic episodes ($NR-PM_1$ reaching up to 68 µg

5   m^{-3} over a 30-min period). PM_1 concentrations were on average 8.2 µg m^{-3} representing 11% of PM_{10}, and were dominated by NR species (71%) with minor contributions of absorbing species (9%). The remaining unaccounted fraction (20% on average, up to 75% during identified dust events) was mainly attributed to mineral dust, strongly suggesting a minor contribution of sea salt in the submicron fraction. Fe concentrations (5%) obtained from the deconvolution of absorption measurements were consistent with the dust events observed on site. Among the species

10   identified in the PM_1 fraction, sulfate and organics represented 32 and 31%, respectively, followed by ammonium 14%, nitrate 9%, BC 5%, Fe 9% and Chl <1%. OM dominated the $NR-PM_1$ fraction when the sampling site was under continental air mass influences (north-eastern winds), whereas marine air masses (from western winds) preferentially brought higher concentrations of sulfate species on site.

Source apportionment of the organic fraction allowed to identify four types of OA. The organic fraction is composed

15   of a highly-oxidized OOA (45%), whose regional origin is underlined by its important contribution to the organic fraction during marine days (62%) but also by its increasing concentration during daytime with a maximum under sea breeze influence. Nonetheless, its higher correlation with NO_3 as well as morning and evening peaks observed for continental and sea breeze daily profiles tend to associate it partially to direct emissions or fast oxidation processes of anthropogenic compounds. Three primary OA linked to anthropogenic activities from nearby sources

20   were also identified: HOA (22%), COA (28%) and a new factor LCOA (3%) related to local combustion sources (emissions from open-waste burning and fish smoking areas), for which a good correlation with particulate chloride (m/z 36) was consistently found. Non-refractory chloride fragments from waste burning or fish smoking areas were suggested to originate from plastic smoldering (for the former) and/or sea salt (for both) submitted to high temperatures. This factor, although minor on average, could represent as high as 7% on a 30-minute time period

25   when the air masses were blowing from the waste burning areas, and very likely resulted in the concomitant emissions of highly-toxic compounds such as dioxins that would require further investigation.

Overall, our study suggests that natural sources strongly influence PM_1 levels in M'Bour, mainly due to the large influence of marine conditions associated with high sulfate levels, and additional significant influence of desert dust. Our measurements carried out at a suburban site away from megacities allowed to provide new insight into the

30   complex mixture between local anthropogenic sources and regional background aerosols in the PM_1 fraction in West Africa at the end of the dry season.

Data availability

35

Atmospheric
Chemistry
and Physics
Discussions

References

Bond, T. C. and Bergstrom, R. W.: Light Absorption by Carbonaceous Particles: An Investigative Review, Aerosol Sci. Technol., 40(1), 27–67, doi:10.1080/02786820500421521, 2006.

10 Bovchaliuk, V., Podvin, T., Mortier, A., Goloub, P., Dubovik, O., Tanré, D., Veselovskii, I. and Victori, S.: Aerosol optical and microphysical properties retrieved from combination LIDAR with sun/sky photometer: preliminary results over Lille, Data Process., 4, 02, 2014.

Brauer, M., Amann, M., Burnett, R. T., Cohen, A., Dentener, F., Ezzati, M., Henderson, S. B., Krzyzanowski, M., Martin, R. V., Van Dingenen, R., van Donkelaar, A. and Thurston, G. D.: Exposure Assessment for Estimation of the
15 Global Burden of Disease Attributable to Outdoor Air Pollution, Environ. Sci. Technol., 46(2), 652–660, doi:10.1021/es2025752, 2012.

Bressi, M., Cavalli, F., Belis, C. A., Putaud, J.-P., Fröhlich, R., Martins dos Santos, S., Petralia, E., Prévôt, A. S. H., Berico, M., Malaguti, A. and Canonaco, F.: Variations in the chemical composition of the submicron aerosol and in the sources of the organic fraction at a regional background site of the Po Valley (Italy), Atmos Chem Phys, 16(20),
20 12875–12896, doi:10.5194/acp-16-12875-2016, 2016.

Brook, R. D., Franklin, B., Cascio, W., Hong, Y., Howard, G., Lipsett, M., Luepker, R., Mittleman, M., Samet, J. and Smith, S. C.: Air pollution and cardiovascular disease A statement for healthcare professionals from the expert panel on population and prevention science of the American Heart Association, Circulation, 109(21), 2655–2671, 2004.

25 Budisulistiorini, S. H., Canagaratna, M. R., Croteau, P. L., Baumann, K., Edgerton, E. S., Kollman, M. S., Ng, N. L., Verma, V., Shaw, S. L., Knipping, E. M., Worsnop, D. R., Jayne, J. T., Weber, R. J. and Surratt, J. D.: Intercomparison of an Aerosol Chemical Speciation Monitor (ACSM) with ambient fine aerosol measurements in downtown Atlanta, Georgia, Atmos Meas Tech, 7(7), 1929–1941, doi:10.5194/amt-7-1929-2014, 2014.

Canagaratna, M. R., Jayne, J. T., Jimenez, J. L., Allan, J. D., Alfarra, M. R., Zhang, Q., Onasch, T. B., Drewnick, F.,
30 Coe, H., Middlebrook, A., Delia, A., Williams, L. R., Trimborn, A. M., Northway, M. J., DeCarlo, P. F., Kolb, C. E., Davidovits, P. and Worsnop, D. R.: Chemical and microphysical characterization of ambient aerosols with the aerodyne aerosol mass spectrometer, Mass Spectrom. Rev., 26(2), 185–222, doi:10.1002/mas.20115, 2007.

Canonaco, F., Crippa, M., Slowik, J. G., Baltensperger, U. and Prévôt, A. S. H.: SoFi, an IGOR-based interface for the efficient use of the generalized multilinear engine (ME-2) for the source apportionment: ME-2 application to
35 aerosol mass spectrometer data, Atmos Meas Tech, 6(12), 3649–3661, doi:10.5194/amt-6-3649-2013, 2013.

Charlson, R. J., Lovelock, J. E., Andreae, M. O. and Warren, S. G.: Oceanic phytoplankton, atmospheric sulphur, cloud albedo and climate, Nature, 326(6114), 655–661, 1987.

Chiapello, I., Bergametti, G., Gomes, L., Chatenet, B., Dulac, F., Pimenta, J. and Suares, E. S.: An additional low layer transport of Sahelian and Saharan dust over the north-eastern Tropical Atlantic, Geophys. Res. Lett., 22(23),
40 3191–3194, doi:10.1029/95GL03313, 1995.

Atmospheric
Chemistry
and Physics
Discussions

Open Access

Chou, C., Formenti, P., Maille, M., Ausset, P., Helas, G., Harrison, M. and Osborne, S.: Size distribution, shape, and composition of mineral dust aerosols collected during the African Monsoon Multidisciplinary Analysis Special Observation Period 0: Dust and Biomass-Burning Experiment field campaign in Niger, January 2006, J. Geophys. Res. Atmospheres, 113(D23), D00C10, doi:10.1029/2008JD009897, 2008.

5 Crenn, V., Sciare, J., Croteau, P. L., Verlhac, S., Fröhlich, R., Belis, C. A., Aas, W., Äijälä, M., Alastuey, A., Artiñano, B., Baisnée, D., Bonnaire, N., Bressi, M., Canagaratna, M., Canonaco, F., Carbone, C., Cavalli, F., Coz, E., Cubison, M. J., Esser-Gietl, J. K., Green, D. C., Gros, V., Heikkinen, L., Herrmann, H., Lunder, C., Minguillón, M. C., Močnik, G., O'Dowd, C. D., Ovadnevaite, J., Petit, J.-E., Petralia, E., Poulain, L., Priestman, M., Riffault, V., Ripoll, A., Sarda-Estève, R., Slowik, J. G., Setyan, A., Wiedensohler, A., Baltensperger, U., Prévôt, A. S. H., Jayne, 10 J. T. and Favez, O.: ACTRIS ACSM intercomparison – Part 1: Reproducibility of concentration and fragment results from 13 individual Quadrupole Aerosol Chemical Speciation Monitors (Q-ACSM) and consistency with co-located instruments, Atmos Meas Tech, 8(12), 5063–5087, doi:10.5194/amt-8-5063-2015, 2015.

Crippa, M., El Haddad, I., Slowik, J. G., DeCarlo, P. F., Mohr, C., Heringa, M. F., Chirico, R., Marchand, N., Sciare, J. and Baltensperger, U.: Identification of marine and continental aerosol sources in Paris using high resolution 15 aerosol mass spectrometry, J. Geophys. Res. Atmospheres, 118(4), 1950–1963, 2013.

Cubison, M. J., Ortega, A. M., Hayes, P. L., Farmer, D. K., Day, D., Lechner, M. J., Brune, W. H., Apel, E., Diskin, G. S., Fisher, J. A., Fuelberg, H. E., Hecobian, A., Knapp, D. J., Mikoviny, T., Riemer, D., Sachse, G. W., Sessions, W., Weber, R. J., Weinheimer, A. J., Wisthaler, A. and Jimenez, J. L.: Effects of aging on organic aerosol from open biomass burning smoke in aircraft and laboratory studies, Atmos Chem Phys, 11(23), 12049–12064, 20 doi:10.5194/acp-11-12049-2011, 2011.

Deboudt, K., Flament, P., Choël, M., Gloter, A., Sobanska, S. and Colliex, C.: Mixing state of aerosols and direct observation of carbonaceous and marine coatings on African dust by individual particle analysis, J. Geophys. Res. Atmospheres, 115(D24), D24207, doi:10.1029/2010jd013921, 2010.

Derimian, Y., Léon, J.-F., Dubovik, O., Chiapello, I., Tanré, D., Sinyuk, A., Auriol, F., Podvin, T., Brogniez, G. and 25 Holben, B. N.: Radiative properties of aerosol mixture observed during the dry season 2006 over M'Bour, Senegal (African Monsoon Multidisciplinary Analysis campaign), J. Geophys. Res. Atmospheres, 113(D23), D00C09, doi:10.1029/2008JD009904, 2008.

Doumbia, E. H. T., Liousse, C., Galy-Lacaux, C., Ndiaye, S. A., Diop, B., Ouafo, M., Assamoi, E. M., Gardrat, E., Castera, P., Rosset, R., Akpo, A. and Sigha, L.: Real time black carbon measurements in West and Central Africa 30 urban sites, Atmos. Environ., 54, 529–537, doi:10.1016/j.atmosenv.2012.02.005, 2012.

Drinovec, L., Močnik, G., Zotter, P., Prévôt, A. S. H., Ruckstuhl, C., Coz, E., Rupakheti, M., Sciare, J., Müller, T., Wiedensohler, A. and Hansen, A. D. A.: The "dual-spot" Aethalometer: an improved measurement of aerosol black carbon with real-time loading compensation, Atmos Meas Tech, 8(5), 1965–1979, doi:10.5194/amt-8-1965-2015, 2015.

35 Du, W., Sun, Y. L., Xu, Y. S., Jiang, Q., Wang, Q. Q., Yang, W., Wang, F., Bai, Z. P., Zhao, X. D. and Yang, Y. C.: Chemical characterization of submicron aerosol and particle growth events at a national background site (3295 m a.s.l.) in the Tibetan Plateau, Atmos Chem Phys Discuss, 15(9), 13515–13550, doi:10.5194/acpd-15-13515-2015, 2015.

Fialho, P., Hansen, A. D. A. and Honrath, R. E.: Absorption coefficients by aerosols in remote areas: a new approach 40 to decouple dust and black carbon absorption coefficients using seven-wavelength Aethalometer data, J. Aerosol Sci., 36(2), 267–282, doi:10.1016/j.jaerosci.2004.09.004, 2005.

Fialho, P., Freitas, M. C., Barata, F., Vieira, B., Hansen, A. D. A. and Honrath, R. E.: The Aethalometer calibration and determination of iron concentration in dust aerosols, J. Aerosol Sci., 37(11), 1497–1506, doi:10.1016/j.jaerosci.2006.03.002, 2006.

Atmospheric
Chemistry
and Physics
Discussions

Fialho, P., Cerqueira, M., Pio, C., Cardoso, J., Nunes, T., Custódio, D., Alves, C., Almeida, S. M., Almeida-Silva, M., Reis, M. and Rocha, F.: The application of a multi-wavelength Aethalometer to estimate iron dust and black carbon concentrations in the marine boundary layer of Cape Verde, Atmos. Environ., 97, 136–143, doi:10.1016/j.atmosenv.2014.08.008, 2014.

5 Fitzgerald, J. W.: Marine aerosols: A review, Atmospheric Environ. Part Gen. Top., 25(3–4), 533–545, doi:10.1016/0960-1686(91)90050-H, 1991.

Flament, P., Deboudt, K., Cachier, H., Châtenet, B. and Mériaux, X.: Mineral dust and carbonaceous aerosols in West Africa: Source assessment and characterization, Atmos. Environ., 45(22), 3742–3749, doi:10.1016/j.atmosenv.2011.04.013, 2011.

10 Fomba, K. W., Müller, K., van Pinxteren, D., Poulain, L., van Pinxteren, M. and Herrmann, H.: Long-term chemical characterization of tropical and marine aerosols at the Cape Verde Atmospheric Observatory (CVAO) from 2007 to 2011, Atmospheric Chem. Phys., 14(17), 8883–8904, doi:10.5194/acp-14-8883-2014, 2014.

Formenti, P., Rajot, J. L., Desboeufs, K., Caquineau, S., Chevaillier, S., Nava, S., Gaudichet, A., Journet, E., Triquet, S., Alfaro, S., Chiari, M., Haywood, J., Coe, H. and Highwood, E.: Regional variability of the composition of
15 mineral dust from western Africa: Results from the AMMA SOP0/DABEX and DODO field campaigns, J. Geophys. Res. Atmospheres, 113(D23), D00C13, doi:10.1029/2008jd009903, 2008a.

Formenti, P., Rajot, J. L., Desboeufs, K., Caquineau, S., Chevaillier, S., Nava, S., Gaudichet, A., Journet, E., Triquet, S., Alfaro, S., Chiari, M., Haywood, J., Coe, H. and Highwood, E.: Regional variability of the composition of mineral dust from western Africa: Results from the AMMA SOP0/DABEX and DODO field campaigns, J. Geophys.
20 Res. Atmospheres, 113(D23), D00C13, doi:10.1029/2008JD009903, 2008b.

Fröhlich, R., Cubison, M. J., Slowik, J. G., Bukowiecki, N., Canonaco, F., Croteau, P. L., Gysel, M., Henne, S., Herrmann, E., Jayne, J. T., Steinbacher, M., Worsnop, D. R., Baltensperger, U. and Prévôt, A. S. H.: Fourteen months of on-line measurements of the non-refractory submicron aerosol at the Jungfraujoch (3580 m a.s.l.) – chemical composition, origins and organic aerosol sources, Atmos Chem Phys, 15(19), 11373–11398,
25 doi:10.5194/acp-15-11373-2015, 2015.

Grover, B. D., Kleinman, M., Eatough, N. L., Eatough, D. J., Hopke, P. K., Long, R. W., Wilson, W. E., Meyer, M. B. and Ambs, J. L.: Measurement of total PM2.5 mass (nonvolatile plus semivolatile) with the Filter Dynamic Measurement System tapered element oscillating microbalance monitor, J. Geophys. Res. Atmospheres, 110(D7), D07S03, doi:10.1029/2004JD004995, 2005.

30 Gullett, B. K., Lemieux, P. M., Lutes, C. C., Winterrowd, C. K. and Winters, D. L.: Emissions of PCDD/F from uncontrolled, domestic waste burning, Chemosphere, 43(4–7), 721–725, doi:10.1016/S0045-6535(00)00425-2, 2001.

Hallquist, M., Wenger, J. C., Baltensperger, U., Rudich, Y., Simpson, D., Claeys, M., Dommen, J., Donahue, N. M., George, C., Goldstein, A. H., Hamilton, J. F., Herrmann, H., Hoffmann, T., Iinuma, Y., Jang, M., Jenkin, M. E., Jimenez, J. L., Kiendler-Scharr, A., Maenhaut, W., McFiggans, G., Mentel, T. F., Monod, A., Prévôt, A. S. H.,
35 Seinfeld, J. H., Surratt, J. D., Szmigielski, R. and Wildt, J.: The formation, properties and impact of secondary organic aerosol: current and emerging issues, Atmospheric Chem. Phys., 9(14), 5155–5236, doi:10.5194/acp-9-5155-2009, 2009.

Hand, V. L., Capes, G., Vaughan, D. J., Formenti, P., Haywood, J. M. and Coe, H. C. D.: Evidence of internal mixing of African dust and biomass burning particles by individual particle analysis using electron beam techniques,
40 J. Geophys. Res. Atmospheres, 115(D13), n/a-n/a, doi:10.1029/2009jd012938, 2010.

Haywood, J. M., Pelon, J., Formenti, P., Bharmal, N., Brooks, M., Capes, G., Chazette, P., Chou, C., Christopher, S., Coe, H., Cuesta, J., Derimian, Y., Desboeufs, K., Greed, G., Harrison, M., Heese, B., Highwood, E. J., Johnson, B., Mallet, M., Marticorena, B., Marsham, J., Milton, S., Myhre, G., Osborne, S. R., Parker, D. J., Rajot, J. L., Schulz, M., Slingo, A., Tanré, D. and Tulet, P.: Overview of the Dust and Biomass-burning Experiment and African

Atmospheric
Chemistry
and Physics
Discussions

Monsoon Multidisciplinary Analysis Special Observing Period-0, J. Geophys. Res. Atmospheres, 113(D23), D00C17, doi:10.1029/2008jd010077, 2008.

Hennigan, C. J., Sullivan, A. P., Collett, J. L. and Robinson, A. L.: Levoglucosan stability in biomass burning particles exposed to hydroxyl radicals, Geophys. Res. Lett., 37(9), L09806, doi:10.1029/2010GL043088, 2010.

5 Holben, B. N., Eck, T. F., Slutsker, I., Tanré, D., Buis, J. P., Setzer, A., Vermote, E., Reagan, J. A., Kaufman, Y. J., Nakajima, T., Lavenu, F., Jankowiak, I. and Smirnov, A.: AERONET—A Federated Instrument Network and Data Archive for Aerosol Characterization, Remote Sens. Environ., 66(1), 1–16, doi:10.1016/S0034-4257(98)00031-5, 1998.

Ianniello, A., Spataro, F., Esposito, G., Allegrini, I., Hu, M. and Zhu, T.: Chemical characteristics of inorganic
10 ammonium salts in $PM_{2.5}$ in the atmosphere of Beijing (China), Atmospheric Chem. Phys., 11(21), 10803–10822, doi:10.5194/acp-11-10803-2011, 2011.

IPCC: Climate change 2007-the physical science basis: Working group I contribution to the fourth assessment report of the IPCC, Cambridge University Press., 2007.

IPCC: Climate Change 2013: The Physical Science Basis: Working Group I Contribution to the Fifth Assessment
15 Report of the Intergovernmental Panel on Climate Change, Cambridge University Press., 2013.

Joshi, N., Romanias, M., Riffault, V. and Thévenet, F.: Investigating water adsorption on natural mineral dust particles: A DRIFT and BET theory study, submitted to Aeolian Research, 2017.

Kaly, F., Marticorena, B., Chatenet, B., Rajot, J. L., Janicot, S., Niang, A., Yahi, H., Thiria, S., Maman, A., Zakou, A., Coulibaly, B. S., Coulibaly, M., Koné, I., Traoré, S., Diallo, A. and Ndiaye, T.: Variability of mineral dust
20 concentrations over West Africa monitored by the Sahelian Dust Transect, Atmospheric Res., 164–165, 226–241, doi:10.1016/j.atmosres.2015.05.011, 2015.

Karol, Y., Tanré, D., Goloub, P., Vervaerde, C., Balois, J. Y., Blarel, L., Podvin, T., Mortier, A. and Chaikovsky, A.: Airborne sun photometer PLASMA: concept, measurements, comparison of aerosol extinction vertical profile with lidar, Atmos Meas Tech, 6(9), 2383–2389, doi:10.5194/amt-6-2383-2013, 2013.

25 Kelly, F. J. and Fussell, J. C.: Size, source and chemical composition as determinants of toxicity attributable to ambient particulate matter, Atmos. Environ., 60, 504–526, 2012.

Lafon, S., Sokolik, I. N., Rajot, J. L., Caquineau, S. and Gaudichet, A.: Characterization of iron oxides in mineral dust aerosols: Implications for light absorption, J. Geophys. Res. Atmospheres, 111(D21), D21207, doi:10.1029/2005JD007016, 2006.

30 Lanz, V. A., Prévôt, A. S. H., Alfarra, M. R., Weimer, S., Mohr, C., DeCarlo, P. F., Gianini, M. F. D., Hueglin, C., Schneider, J., Favez, O., D'Anna, B., George, C. and Baltensperger, U.: Characterization of aerosol chemical composition with aerosol mass spectrometry in Central Europe: an overview, Atmos Chem Phys, 10(21), 10453–10471, doi:10.5194/acp-10-10453-2010, 2010.

Lemieux, P. M., Lutes, C. C. and Santoianni, D. A.: Emissions of organic air toxics from open burning: a
35 comprehensive review, Prog. Energy Combust. Sci., 30(1), 1–32, doi:10.1016/j.pecs.2003.08.001, 2004.

Léon, J.-F., Derimian, Y., Chiapello, I., Tanré, D., Podvin, T., Chatenet, B., Diallo, A. and Deroo, C.: Aerosol vertical distribution and optical properties over M'Bour (16.96° W; 14.39° N), Senegal from 2006 to 2008, Atmos Chem Phys, 9(23), 9249–9261, doi:10.5194/acp-9-9249-2009, 2009.

Liousse, C., Guillaume, B., Grégoire, J. M., Mallet, M., Galy, C., Pont, V., Akpo, A., Bedou, M., Castéra, P.,
40 Dungall, L., Gardrat, E., Granier, C., Konaré, A., Malavelle, F., Mariscal, A., Mieville, A., Rosset, R., Serça, D., Solmon, F., Tummon, F., Assamoi, E., Yoboué, V. and Van Velthoven, P.: Updated African biomass burning

emission inventories in the framework of the AMMA-IDAF program, with an evaluation of combustion aerosols, Atmos Chem Phys, 10(19), 9631–9646, doi:10.5194/acp-10-9631-2010, 2010.

Marticorena, B., Chatenet, B., Rajot, J. L., Traoré, S., Coulibaly, M., Diallo, A., Koné, I., Maman, A., Ndiaye, T. and Zakou, A.: Temporal variability of mineral dust concentrations over West Africa: analyses of a pluriannual monitoring from the AMMA Sahelian Dust Transect, Atmos Chem Phys, 10(18), 8899–8915, doi:10.5194/acp-10-8899-2010, 2010.

Martiny, N. and Chiapello, I.: Assessments for the impact of mineral dust on the meningitis incidence in West Africa, Atmos. Environ., 70(0), 245–253, doi:10.1016/j.atmosenv.2013.01.016, 2013.

McCulloch, A., Aucott, M. L., Benkovitz, C. M., Graedel, T. E., Kleiman, G., Midgley, P. M. and Li, Y.-F.: Global emissions of hydrogen chloride and chloromethane from coal combustion, incineration and industrial activities: Reactive Chlorine Emissions Inventory, J. Geophys. Res. Atmospheres, 104(D7), 8391–8403, doi:10.1029/1999JD900025, 1999.

Middlebrook, A. M., Bahreini, R., Jimenez, J. L. and Canagaratna, M. R.: Evaluation of Composition-Dependent Collection Efficiencies for the Aerodyne Aerosol Mass Spectrometer using Field Data, Aerosol Sci. Technol., 46(3), 258–271, doi:10.1080/02786826.2011.620041, 2012.

Milic, A., Mallet, M. D., Cravigan, L. T., Alroe, J., Ristovski, Z. D., Selleck, P., Lawson, S. J., Ward, J., Desservettaz, M. J., Paton-Walsh, C., Williams, L. R., Keywood, M. D. and Miljevic, B.: Aging of aerosols emitted from biomass burning in northern Australia, Atmos Chem Phys Discuss, 2016, 1–24, doi:10.5194/acp-2016-730, 2016.

Minguillón, M., Ripoll, A., Pérez, N., Prévôt, A., Canonaco, F., Querol, X. and Alastuey, A.: Chemical characterization of submicron regional background aerosols in the Western Mediterranean using an Aerosol Chemical Speciation Monitor, Atmospheric Chem. Phys. Discuss., 15(1), 965–1000, 2015.

Mohr, C., DeCarlo, P. F., Heringa, M. F., Chirico, R., Slowik, J. G., Richter, R., Reche, C., Alastuey, A., Querol, X., Seco, R., Peñuelas, J., Jiménez, J. L., Crippa, M., Zimmermann, R., Baltensperger, U. and Prévôt, A. S. H.: Identification and quantification of organic aerosol from cooking and other sources in Barcelona using aerosol mass spectrometer data, Atmos Chem Phys, 12(4), 1649–1665, doi:10.5194/acp-12-1649-2012, 2012.

Moreno, T., Querol, X., Castillo, S., Alastuey, A., Cuevas, E., Herrmann, L., Mounkaila, M., Elvira, J. and Gibbons, W.: Geochemical variations in aeolian mineral particles from the Sahara–Sahel Dust Corridor, Chemosphere, 65(2), 261–270, doi:10.1016/j.chemosphere.2006.02.052, 2006.

Ng, N. L., Herndon, S. C., Trimborn, A., Canagaratna, M. R., Croteau, P. L., Onasch, T. B., Sueper, D., Worsnop, D. R., Zhang, Q., Sun, Y. L. and Jayne, J. T.: An Aerosol Chemical Speciation Monitor (ACSM) for Routine Monitoring of the Composition and Mass Concentrations of Ambient Aerosol, Aerosol Sci. Technol., 45(7), 780–794, doi:10.1080/02786826.2011.560211, 2011a.

Ng, N. L., Canagaratna, M. R., Jimenez, J. L., Zhang, Q., Ulbrich, I. M. and Worsnop, D. R.: Real-Time Methods for Estimating Organic Component Mass Concentrations from Aerosol Mass Spectrometer Data, Environ. Sci. Technol., 45(3), 910–916, doi:10.1021/es102951k, 2011b.

Nuaaman, I., Li, S.-M., Hayden, K. L., Onasch, T. B., Massoli, P., Sueper, D., Worsnop, D. R., Bates, T. S., Quinn, P. K. and McLaren, R.: Separating refractory and non-refractory particulate chloride and estimating chloride depletion by aerosol mass spectrometry in a marine environment, Atmos Chem Phys Discuss, 15(2), 2085–2118, doi:10.5194/acpd-15-2085-2015, 2015.

Osborne, S. R., Johnson, B. T., Haywood, J. M., Baran, A. J., Harrison, M. A. J. and McConnell, C. L.: Physical and optical properties of mineral dust aerosol during the Dust and Biomass-burning Experiment, J. Geophys. Res. Atmospheres, 113(D23), D00C03, doi:10.1029/2007jd009551, 2008.

Ovadnevaite, J., Ceburnis, D., Canagaratna, M., Berresheim, H., Bialek, J., Martucci, G., Worsnop, D. R. and O'Dowd, C.: On the effect of wind speed on submicron sea salt mass concentrations and source fluxes, J. Geophys. Res. Atmospheres, 117(D16), D16201, doi:10.1029/2011JD017379, 2012.

5   Paatero, P. and Tapper, U.: Positive matrix factorization: A non-negative factor model with optimal utilization of error estimates of data values, Environmetrics, 5(2), 111–126, doi:10.1002/env.3170050203, 1994.

Paris, R., Desboeufs, K. V., Formenti, P., Nava, S. and Chou, C.: Chemical characterisation of iron in dust and biomass burning aerosols during AMMA-SOP0/DABEX: implication for iron solubility, Atmospheric Chem. Phys., 10(9), 4273–4282, doi:10.5194/acp-10-4273-2010, 2010.

Parworth, C., Fast, J., Mei, F., Shippert, T., Sivaraman, C., Tilp, A., Watson, T. and Zhang, Q.: Long-term
10 measurements of submicrometer aerosol chemistry at the Southern Great Plains (SGP) using an Aerosol Chemical Speciation Monitor (ACSM), Atmos. Environ., 106, 43–55, doi:10.1016/j.atmosenv.2015.01.060, 2015.

Petit, J.-E., Favez, O., Sciare, J., Canonaco, F., Croteau, P., Močnik, G., Jayne, J., Worsnop, D. and Leoz-Garziandia, E.: Submicron aerosol source apportionment of wintertime pollution in Paris, France by double positive matrix factorization (PMF2) using an aerosol chemical speciation monitor (ACSM) and a multi-wavelength Aethalometer,
15 Atmos Chem Phys, 14(24), 13773–13787, doi:10.5194/acp-14-13773-2014, 2014.

Petit, J.-E., Favez, O., Sciare, J., Crenn, V., Sarda-Estève, R., Bonnaire, N., Močnik, G., Dupont, J.-C., Haeffelin, M. and Leoz-Garziandia, E.: Two years of near real-time chemical composition of submicron aerosols in the region of Paris using an Aerosol Chemical Speciation Monitor (ACSM) and a multi-wavelength Aethalometer, Atmos Chem Phys, 15(6), 2985–3005, doi:10.5194/acp-15-2985-2015, 2015.

20 Pio, C. A., Cardoso, J., Cerqueira, M. A., Calvo, A., Nunes, T. V., Alves, C. A., Custodio, D., Almeida, S. M. and Silva, M. A.: Seasonal variability of aerosol concentration and size distribution in Cape Verde using a continuous aerosol optical spectrometer, Front. Environ. Sci., 2, doi:10.3389/fenvs.2014.00015, 2014.

Prenni, A. J., Day, D. E., Evanoski-Cole, A. R., Sive, B. C., Hecobian, A., Zhou, Y., Gebhart, K. A., Hand, J. L., Sullivan, A. P., Li, Y., Schurman, M. I., Desyaterik, Y., Malm, W. C., Collett Jr., J. L. and Schichtel, B. A.: Oil and
25 gas impacts on air quality in federal lands in the Bakken region: an overview of the Bakken Air Quality Study and first results, Atmos Chem Phys, 16(3), 1401–1416, doi:10.5194/acp-16-1401-2016, 2016.

Redelsperger, J.-L., Thorncroft, C. D., Diedhiou, A., Lebel, T., Parker, D. J. and Polcher, J.: African Monsoon Multidisciplinary Analysis: An International Research Project and Field Campaign, Bull. Am. Meteorol. Soc., 87(12), 1739–1746, doi:10.1175/BAMS-87-12-1739, 2006.

30 Ripoll, A., Minguillón, M. C., Pey, J., Jimenez, J. L., Day, D. A., Sosedova, Y., Canonaco, F., Prévôt, A. S. H., Querol, X. and Alastuey, A.: Long-term real-time chemical characterization of submicron aerosols at Montsec (southern Pyrenees, 1570 m a.s.l.), Atmos Chem Phys, 15(6), 2935–2951, doi:10.5194/acp-15-2935-2015, 2015.

Robinson, A. L., Donahue, N. M., Shrivastava, M. K., Weitkamp, E. A., Sage, A. M., Grieshop, A. P., Lane, T. E., Pierce, J. R. and Pandis, S. N.: Rethinking Organic Aerosols: Semivolatile Emissions and Photochemical Aging,
35 Science, 315(5816), 1259–1262, doi:10.1126/science.1133061, 2007.

Salcedo, D., Onasch, T. B., Dzepina, K., Canagaratna, M. R., Zhang, Q., Huffman, J. A., DeCarlo, P. F., Jayne, J. T., Mortimer, P., Worsnop, D. R., Kolb, C. E., Johnson, K. S., Zuberi, B., Marr, L. C., Volkamer, R., Molina, L. T., Molina, M. J., Cardenas, B., Bernabé, R. M., Márquez, C., Gaffney, J. S., Marley, N. A., Laskin, A., Shutthanandan, V., Xie, Y., Brune, W., Lesher, R., Shirley, T. and Jimenez, J. L.: Characterization of ambient aerosols in Mexico
40 City during the MCMA-2003 campaign with Aerosol Mass Spectrometry: results from the CENICA Supersite, Atmos Chem Phys, 6(4), 925–946, doi:10.5194/acp-6-925-2006, 2006.

Schlag, P., Kiendler-Scharr, A., Blom, M. J., Canonaco, F., Henzing, J. S., Moerman, M. M., Prévôt, A. S. H. and Holzinger, R.: Aerosol source apportionment from 1 year measurements at the CESAR tower at Cabauw, NL, Atmos Chem Phys Discuss, 15(23), 35117–35155, doi:10.5194/acpd-15-35117-2015, 2015.

Atmospheric
Chemistry
and Physics
Discussions

Schurman, M. I., Lee, T., Desyaterik, Y., Schichtel, B. A., Kreidenweis, S. M. and Collett Jr., J. L.: Transport, biomass burning, and in-situ formation contribute to fine particle concentrations at a remote site near Grand Teton National Park, Atmos. Environ., 112, 257–268, doi:10.1016/j.atmosenv.2015.04.043, 2015.

5 Slingo, A., Bharmal, N. A., Robinson, G. J., Settle, J. J., Allan, R. P., White, H. E., Lamb, P. J., Lélé, M. I., Turner, D. D., McFarlane, S., Kassianov, E., Barnard, J., Flynn, C. and Miller, M.: Overview of observations from the RADAGAST experiment in Niamey, Niger: Meteorology and thermodynamic variables, J. Geophys. Res. Atmospheres, 113(D13), D00E01, doi:10.1029/2008JD009909, 2008.

Sun, C., Lee, B. P., Huang, D., Jie Li, Y., Schurman, M. I., Louie, P. K. K., Luk, C. and Chan, C. K.: Continuous measurements at the urban roadside in an Asian megacity by Aerosol Chemical Speciation Monitor (ACSM):
10 particulate matter characteristics during fall and winter seasons in Hong Kong, Atmos Chem Phys, 16(3), 1713–1728, doi:10.5194/acp-16-1713-2016, 2016.

Sun, Y., Wang, Z., Dong, H., Yang, T., Li, J., Pan, X., Chen, P. and Jayne, J. T.: Characterization of summer organic and inorganic aerosols in Beijing, China with an Aerosol Chemical Speciation Monitor, Atmos. Environ., 51(0), 250–259, doi:10.1016/j.atmosenv.2012.01.013, 2012.

15 Sun, Y. L., Wang, Z. F., Fu, P. Q., Yang, T., Jiang, Q., Dong, H. B., Li, J. and Jia, J. J.: Aerosol composition, sources and processes during wintertime in Beijing, China, Atmospheric Chem. Phys., 13(9), 4577–4592, doi:10.5194/acp-13-4577-2013, 2013.

Tiitta, P., Vakkari, V., Croteau, P., Beukes, J. P., van Zyl, P. G., Josipovic, M., Venter, A. D., Jaars, K., Pienaar, J. J., Ng, N. L., Canagaratna, M. R., Jayne, J. T., Kerminen, V. M., Kokkola, H., Kulmala, M., Laaksonen, A., Worsnop,
20 D. R. and Laakso, L.: Chemical composition, main sources and temporal variability of PM1 aerosols in southern African grassland, Atmos Chem Phys, 14(4), 1909–1927, doi:10.5194/acp-14-1909-2014, 2014.

Titos, G., Lyamani, H., Pandolfi, M., Alastuey, A. and Alados-Arboledas, L.: Identification of fine (PM1) and coarse (PM10-1) sources of particulate matter in an urban environment, Atmos. Environ., 89(0), 593–602, doi:10.1016/j.atmosenv.2014.03.001, 2015.

25 Topping, D., Coe, H., McFiggans, G., Burgess, R., Allan, J., Alfarra, M. R., Bower, K., Choularton, T. W., Decesari, S. and Facchini, M. C.: Aerosol chemical characteristics from sampling conducted on the Island of Jeju, Korea during ACE Asia, Atmos. Environ., 38(14), 2111–2123, doi:10.1016/j.atmosenv.2004.01.022, 2004.

Tue, N. M., Goto, A., Takahashi, S., Itai, T., Asante, K. A., Kunisue, T. and Tanabe, S.: Release of chlorinated, brominated and mixed halogenated dioxin-related compounds to soils from open burning of e-waste in Agbogbloshie
30 (Accra, Ghana), J. Hazard. Mater., 302, 151–157, doi:10.1016/j.jhazmat.2015.09.062, 2016.

Val, S., Liousse, C., Doumbia, E. H. T., Galy-Lacaux, C., Cachier, H., Marchand, N., Badel, A., Gardrat, E., Sylvestre, A. and Baeza-Squiban, A.: Physico-chemical characterization of African urban aerosols (Bamako in Mali and Dakar in Senegal) and their toxic effects in human bronchial epithelial cells: description of a worrying situation, Part Fibre Toxicol, 10(10), 2013.

35 Veselovskii, I., Goloub, P., Podvin, T., Bovchaliuk, V., Derimian, Y., Augustin, P., Fourmentin, M., Tanre, D., Korenskiy, M., Whiteman, D. N., Diallo, A., Ndiaye, T., Kolgotin, A. and Dubovik, O.: Study of African Dust with multi-wavelength Raman Lidar during the "SHADOW" campaign in Senegal, Atmospheric Chem. Phys. Discuss., 1–40, doi:10.5194/acp-2016-109, 2016.

Von der Weiden, S.-L., Drewnick, F. and Borrmann, S.: Particle Loss Calculator – a new software tool for the
40 assessment of the performance of aerosol inlet systems, Atmos Meas Tech, 2(2), 479–494, doi:10.5194/amt-2-479-2009, 2009.

Weingartner, E., Saathoff, H., Schnaiter, M., Streit, N., Bitnar, B. and Baltensperger, U.: Absorption of light by soot particles: determination of the absorption coefficient by means of aethalometers, J. Aerosol Sci., 34(10), 1445–1463, doi:10.1016/S0021-8502(03)00359-8, 2003.

Zhang, Q., Worsnop, D. R., Canagaratna, M. R. and Jimenez, J. L.: Hydrocarbon-like and oxygenated organic aerosols in Pittsburgh: insights into sources and processes of organic aerosols, Atmospheric Chem. Phys., 5(12), 3289–3311, doi:10.5194/acp-5-3289-2005, 2005.

5   Zhang, Q., Jimenez, J. L., Canagaratna, M. R., Allan, J. D., Coe, H., Ulbrich, I., Alfarra, M. R., Takami, A., Middlebrook, A. M., Sun, Y. L., Dzepina, K., Dunlea, E., Docherty, K., DeCarlo, P. F., Salcedo, D., Onasch, T., Jayne, J. T., Miyoshi, T., Shimono, A., Hatakeyama, S., Takegawa, N., Kondo, Y., Schneider, J., Drewnick, F., Borrmann, S., Weimer, S., Demerjian, K., Williams, P., Bower, K., Bahreini, R., Cottrell, L., Griffin, R. J., Rautiainen, J., Sun, J. Y., Zhang, Y. M. and Worsnop, D. R.: Ubiquity and dominance of oxygenated species in organic aerosols in anthropogenically-influenced Northern Hemisphere midlatitudes, Geophys. Res. Lett., 34(13),
10   L13801, doi:10.1029/2007GL029979, 2007.

Zhang, S., Riffault, V., Dusanter, S., Augustin, P., Fourmentin, M. and Delbarre, H.: One year of real-time chemical speciation measurements of submicron particulate matter (PM1) at a French coastal site: assessment of industrial and shipping emissions, in prep, n.d.

Zhang, Y., Wang, X., Chen, H., Yang, X., Chen, J. and Allen, J. O.: Source apportionment of lead-containing aerosol
15   particles in Shanghai using single particle mass spectrometry, Chemosphere, 74(4), 501–507, doi:10.1016/j.chemosphere.2008.10.004, 2009.

Table 1. Averaged NR-PM1 concentrations (in µg m-3) - with maximum in parentheses when available - and respective contributions of NR compounds for this study compared to other ACSM campaigns from different locations.

| NR-PM$_1$ avg (µg m^{-3})	OM	SO$_4$	NO$_3$	NH$_4$	Chl	Period	Location	Type of site	Reference
50.0	40	18	25	16	<1	Jun. - Aug. 2011	Beijing (China)	Urban	Sun et al. (2012)
25.9	58	23	7	11	<1	Sept.-Dec. 2015	Hong Kong (China)	Urban	Sun et al. (2016)
15.7 (80)	~44	~6	~38	~11	~1	Jan. - Mar. 2012	Paris (France)	Suburban	Petit et al. (2014)
15.3	72	15	6	8	< 1	Summer - Fall 2011	Atlanta (USA)	Urban	Budisulistiorini et al. (2014)
14.2	58	12	21	8	1	Mar. 2013 – Mar 2014	Ispra (Italy)	Rural background	Bressi et al. (2016)
10.8 (~75)	45	30	11	13	1	Sept. - Oct. 2013	Menyuan, Tibetan Plateau (China)	Rural	Du et al. (2015)
9	31	12	41	14	2	Jul. 2012 -Jun. 2013	Cabauw (The Netherlands)	Rural	Schlag et al. (2015)
7.5 (89)	48	32	7	13	<1	Sept. 2010 - Aug. 2011	Welgegund (South Africa)	Rural	Tiitta et al. (2014)
7.2	52	29	7	12	< 1	Jul. - Sept 2010	New-York (USA)	Urban	Ng et al. (2011)
7.0	57	12	21	9	< 1	Nov. 2010 - Jun. 2012	Southern Great plains (USA)	Rural	Parworth et al. (2015)
~7.0	54	19	11	11	< 5	Jun. 2012 - Jul. 2013	Montseny (Spain)	Rural	Minguillón et al. (2015)
5.4 (68.3)	39	35	9	15	<1	Mar. - Jun. 2015	M'Bour (Senegal)	Suburban	This study
4.9	53	25	7	12	< 1	Jul. 2011 - Apr. 2012	Montsec (Spain)	Rural	Ripoll et al. (2015)
0.3 (9.6)	43	30	7	17	/	Oct. 2012 - Oct. 2013	Jungfraujoch (Switzerland)	Rural	Fröhlich et al. (2015)
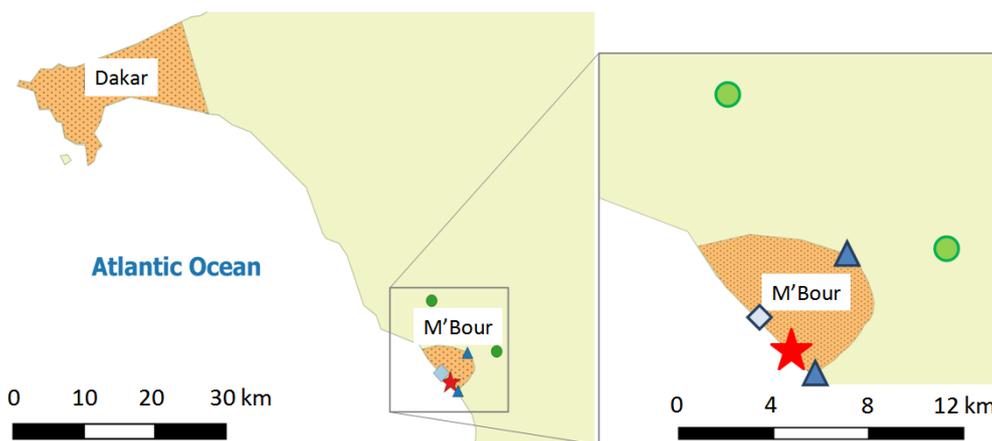
Fig. 1. (left) Dakar and M'Bour locations with city delimitations in orange and (right) local sources located around the IRD sampling site (red star), with open waste burning areas (green circles), fish-smoking sites (blue triangles) and the M'Bour port (light blue diamond).
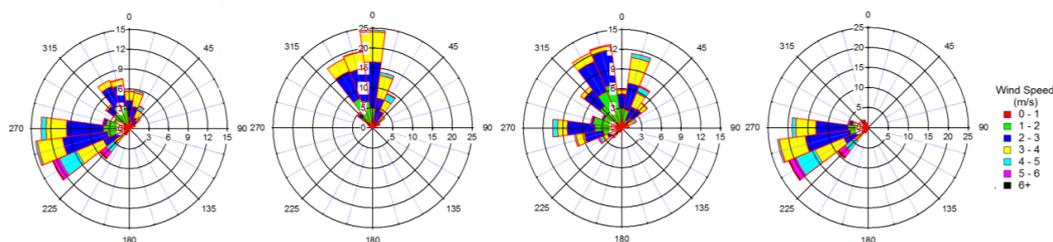
Fig. 2. Rose plots of wind direction divided into 15° sectors and averaged on 30 minutes (ACSM time step) with wind frequencies as radius (in %) and colored by wind speed intervals measured in M'Bour for (a) the whole dataset, (b) days classified as continental (n = 17), (c) sea breeze (n = 29) and (d) marine (n = 45).
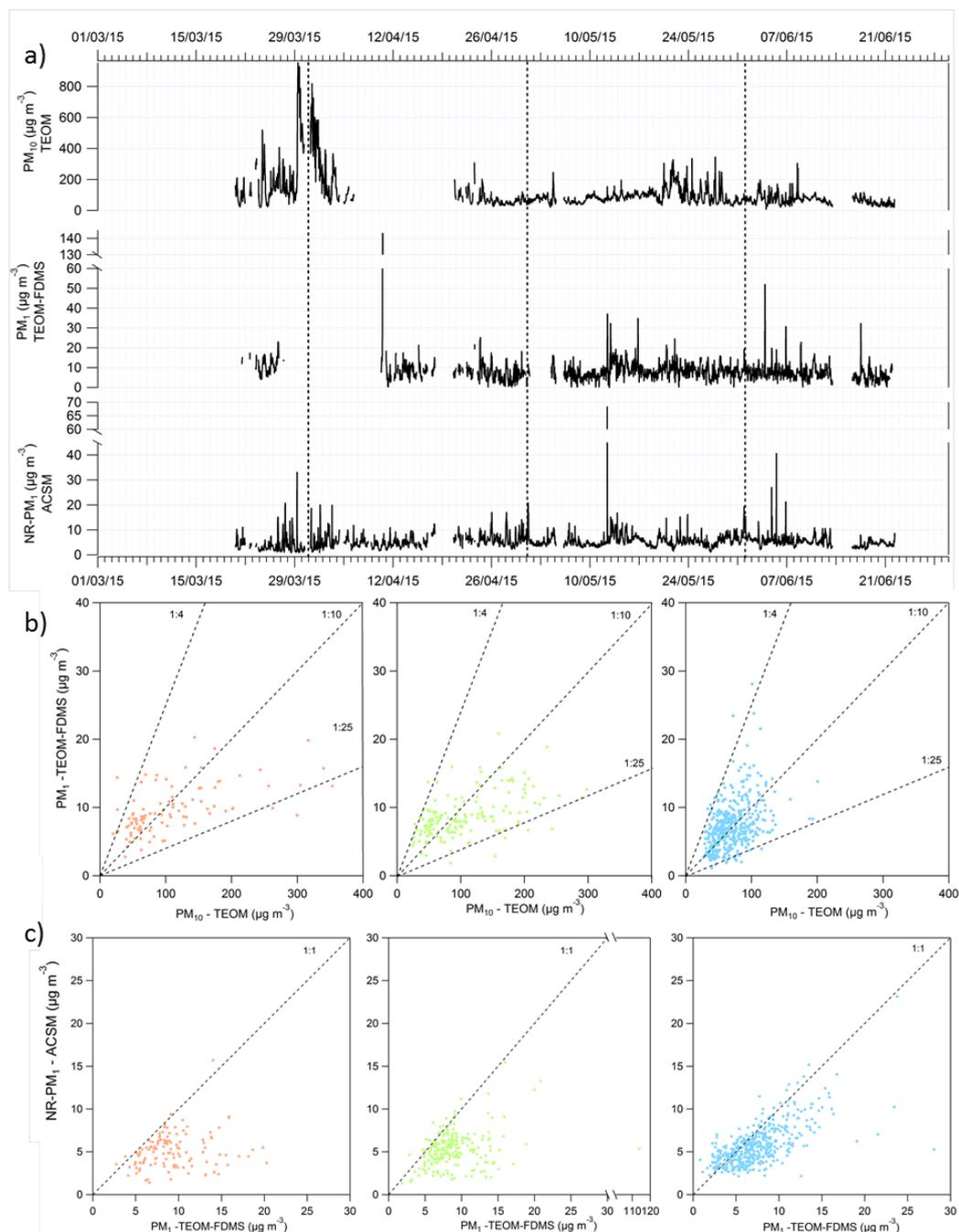
Fig. 3. (a) NR-PM$_1$, total PM$_1$ and PM$_{10}$ time series (30-minute averages) measured over IOP-1, **(b)** 2h averaged scatter plots of total PM$_1$ vs PM$_{10}$ and **(c)** NR-PM$_1$ vs PM$_1$ for (left) continental, (middle) sea breeze and (right) marine days (dotted lines are visual markers representing ratios between the different variables).
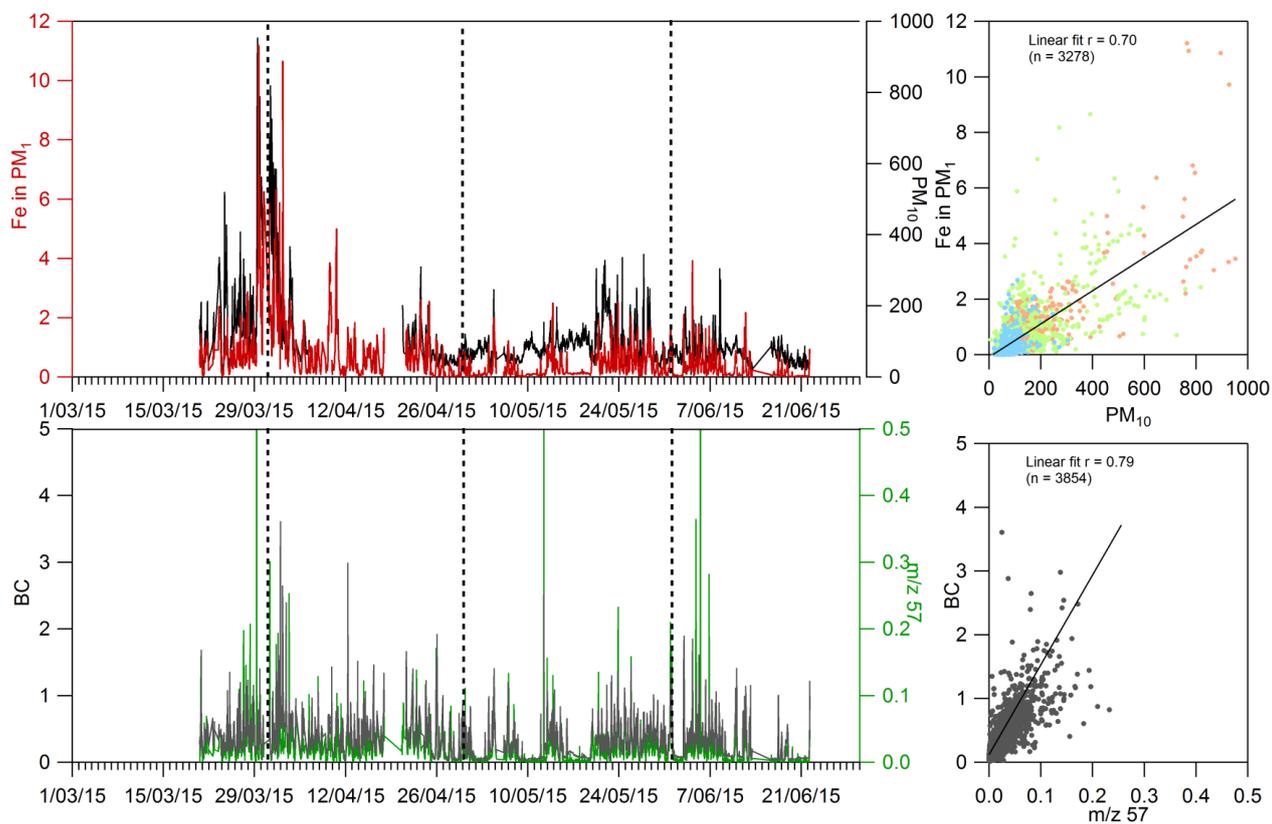
Fig. 4. (Left) Time series of (top) Fe and PM_{10} concentrations (in µg m^{-3}) and (bottom) BC concentration (in µg m^{-3}) and m/z 57 (ng m^{-3}) 30 min average. **(Right)** Corresponding scatter plots and their respective linear fits with Fe and PM_{10} data colored in red for continental, green for sea breeze and blue for marine days and BC and m/z 57 in grey dots.

Atmospheric
Chemistry
and Physics
Discussions
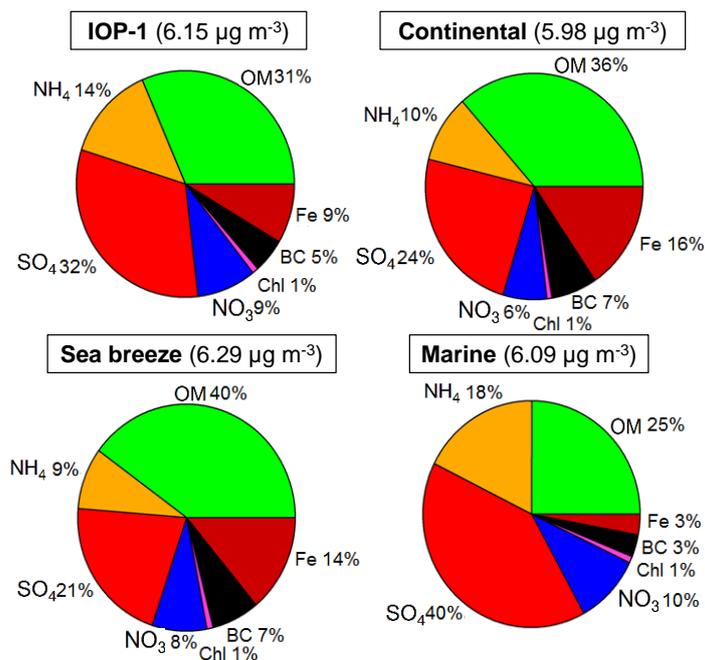
Fig. 5. Averaged contributions of NR-PM$_1$, BC and Fe for IOP-1 (n = 3771), continental (n = 307), sea breeze (n= 799) and marine days (n = 1843) (with average total concentration in µg m^{-3} in parenthesis).
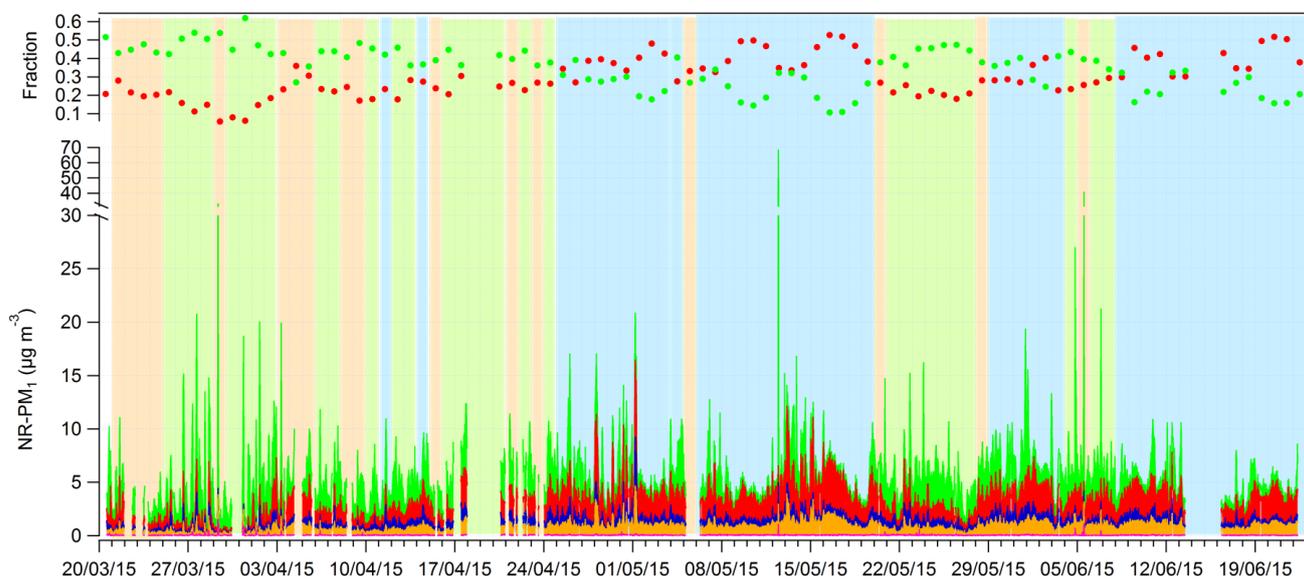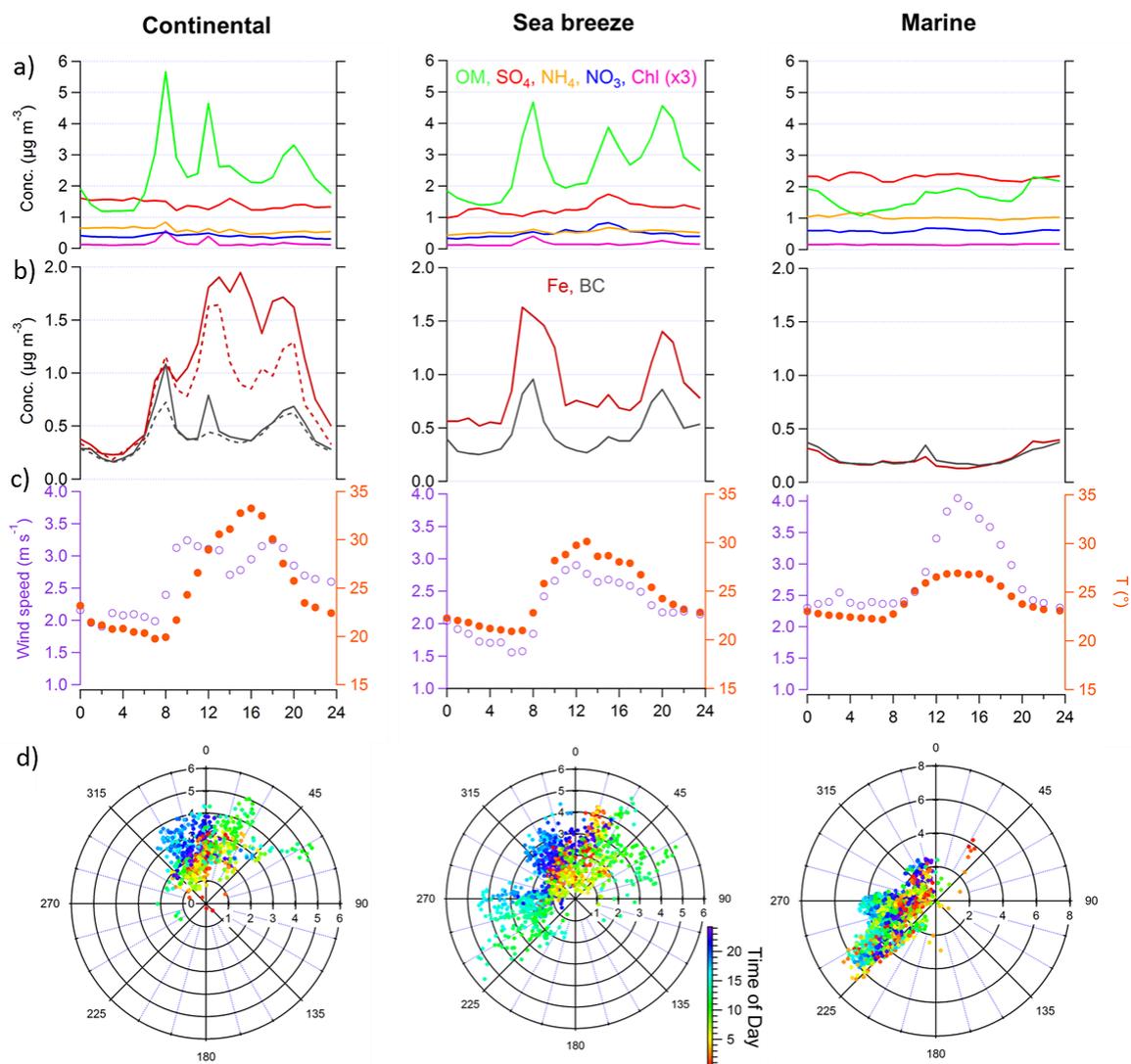
Fig. 6. (Bottom) IOP-1 stacked time series of OM (green), SO₄ (red), NO₃ (blue), NH₄ (orange) and Chl (pink) on ACSM time step (30 min) and **(top)** daily averaged fraction of OM and SO₄. Tinted areas correspond to continental days in light pink, sea breeze days in light green and marine days in light blue.

Fig.7. Average daily profiles of (a) NR-PM₁, (b) BC and Fe concentrations, (c) wind speed and temperature for (from left to right) continental (dotted lines: medians), sea breeze and marine days. (d) Associated wind roses (radius, wind speed in m s-1) colored by time of day in UTC.

Atmospheric
Chemistry
and Physics
Discussions
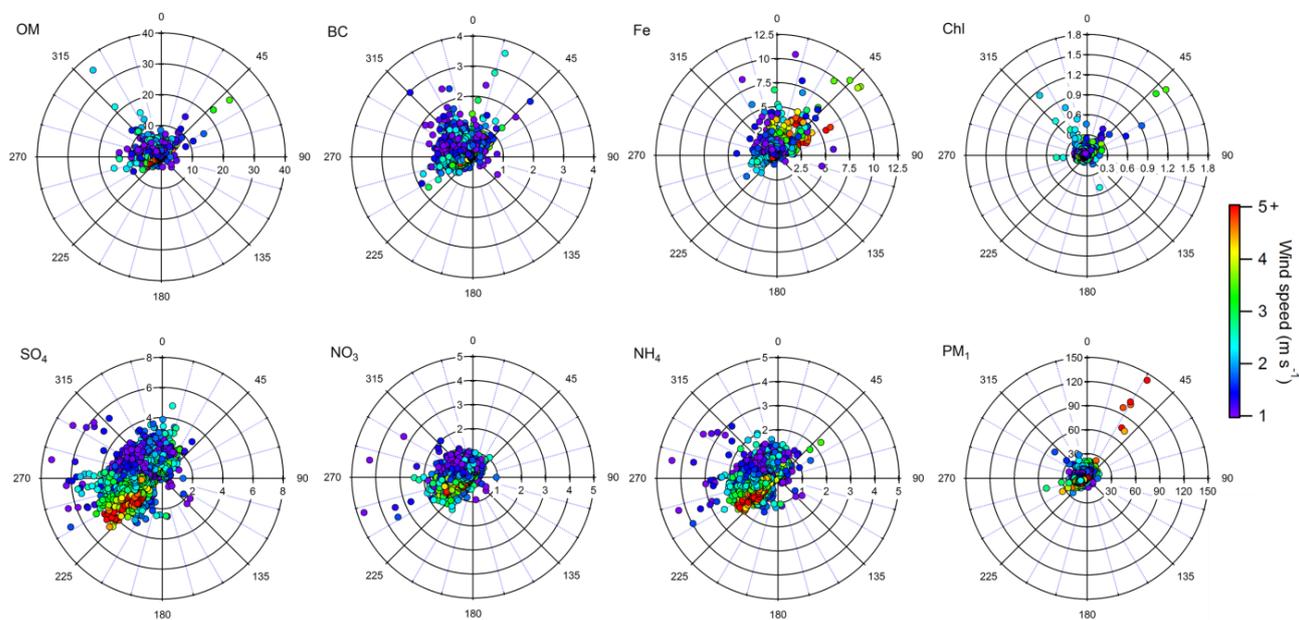
Fig. 8. Pollution rose plots of OM, BC, Chl, Fe, SO$_4$, NO$_3$, NH$_4$ and total PM$_1$ for the whole IOP-1, with concentrations (µg m^{-3}) as radius and colored by wind speed (measurements inferior to 1 m s^{-1} in grey).
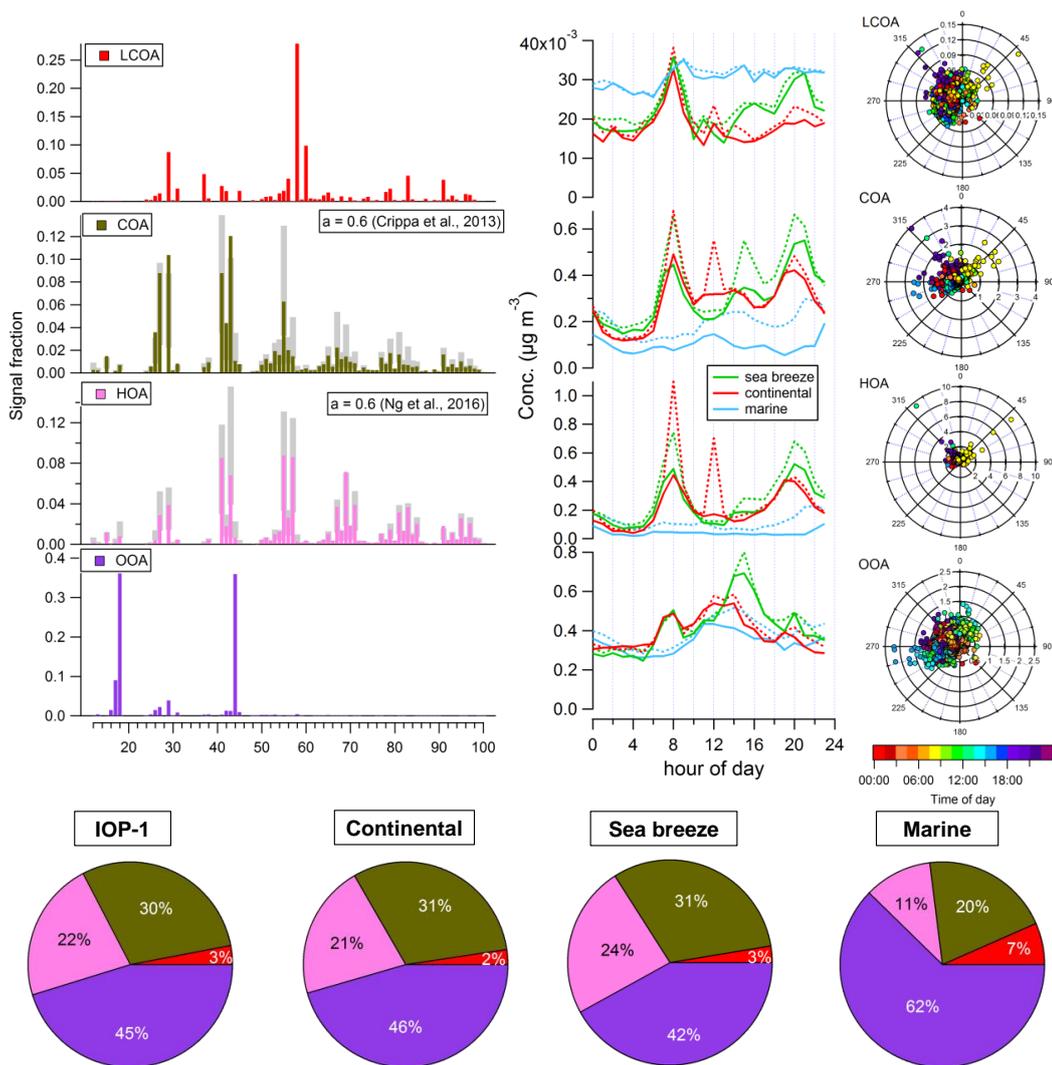
Fig. 9. PMF constrained 4-factor solution: (left) factor profiles of LCOA, COA, HOA (the two latter constrained), OOA; (middle) corresponding daily cycles according to day types (solid lines: median; dotted lines: average); and (right) pollution rose plots colored by time of day. (bottom) Average pie charts of the contributions to the total organic fraction for IOP-1, continental, sea breeze and marine days.